SMYD5 is a novel epigenetic gatekeeper of the mild hypothermia response

Salvor Rafnsdottir[1], Kijin Jang[1], Sara Tholl Halldorsdottir[1], Arnhildur Tomasdottir[1], Meghna Vinod[1], Katrin Möller[1], Tinna Reynisdottir[1], Laufey Halla Atladottir[1], Kristin Elisabet Allison[2], Jin He[3], Li Zhang[4], Frances J. Northington[5], Raul Chavez-Valdez[5], Kimberley Jade Anderson[1], Hans Tomas Bjornsson[1,4,6,7*]

[1]Louma G. Laboratory of Epigenetic Research, Faculty of Medicine, University of Iceland, Reykjavik, Iceland; [2]Faculty of Life and Environmental Sciences, University of Iceland, Reykjavik, Iceland; [3]Department of Biochemistry and Molecular Biology, College of Natural Science, Michigan State University, MI, USA; [4]McKusick-Nathans Department of Genetic Medicine, Johns Hopkins University School of Medicine, MD, USA; [5]Division of Neonatology, Department of Pediatrics, Johns Hopkins University School of Medicine, Baltimore, MD, USA; [6]Department of Pediatrics, Johns Hopkins University, MD, USA; [7]Department of Genetics and Molecular Medicine, Landspitali University Hospital, Reykjavik, Iceland.

***Corresponding author:** Hans Tomas Bjornsson, htb@hi.is

Summary

Organisms have homeostatic mechanisms to respond to cold temperature to ensure survival including the activation of the mammalian neuroprotective mild hypothermia response (MHR) at 32°C. We show activation of the MHR at euthermia by an FDA-approved medication Entacapone, proof-of-principle that the MHR can be medically manipulated. Utilizing a forward CRISPR-Cas9 mutagenesis screen, we identify the histone lysine methyltransferase SMYD5 as an epigenetic gatekeeper of the MHR. SMYD5 represses the key MHR gene *SP1* at euthermia but not at 32°C. This repression is mirrored by temperature-dependent levels of H3K36me3 at the *SP1*-locus and globally indicating that the mammalian MHR is regulated at the level of histone modifications. We identified 45 additional SMYD5-temperature dependent genes suggesting a broader MHR-related role for SMYD5. Our study provides an example of how the epigenetic machinery integrates environmental cues into the genetic circuitry of mammalian cells and suggests novel therapeutic avenues for neuroprotection after catastrophic events.

Keywords: Targeted Temperature Management, SP1, Hypothermia, Neonatal Hypoxic-Ischemic Brain Injury, Cardiac Arrest

32 **Introduction**

33 The defining feature of mammals is their ability to maintain a euthermic body temperature
34 (37°C) and most mammals maintain temperature at a relatively tight range to ensure normal cellular
35 homeostasis[1]. The main exception is the hibernation of some mammals, which is a type of controlled
36 temperature decrease during times of prolonged inactivity[2]. In clinical practice, physicians imitate
37 hibernation with the use of Targeted Temperature Management (TTM) as a therapeutic strategy to
38 minimize neurological damage following neonatal hypoxic-ischemic brain injury and cardiac arrest[3,4].
39 The reasons why lowered internal core temperature (32-36°C) yields benefits are currently not fully
40 understood[5,6]. Although some argue that the positive neurological benefit from mild hypothermia
41 relates to a lower metabolic rate, others point out that the specific upregulation of several genes
42 during mild hypothermia does not fit that idea[7]. An alternative hypothesis is that hypothermia is
43 beneficial because of the activation of the mild hypothermia response (MHR) itself, and if so, it would
44 be important for researchers and clinicians to understand both the mechanisms and the extent of the
45 response. In support of this, researchers have found that several genes (e.g., *CIRBP/CIRP*, *RBM3*)
46 consistently show increased expression during mild hypothermia.[8] Two of these, *SP1* and *RBM3,*
47 appear to have roles in decreasing neuronal death during disease states[9–13].

48 SP1, a transcription factor for many genes[14], binds to the promoter region of *CIRBP*[15] upon
49 cold exposure at a sequence called the Mild Cold Response Element (MCRE)[15], and its binding leads
50 to increased expression of *CIRBP* at 32°C, indicating that this regulation occurs at the transcriptional
51 level[15]. Similarly, RBM3 is known to regulate at least one downstream gene, *RTN3*[11], a potential
52 neuroprotective factor in a neurodegeneration model[11]. Although this suggests that mammalian cells
53 have a pathway culminating in SP1/CIRBP and RBM3/RTN3, little has been done to further elucidate
54 the upstream regulation of this pathway and relatively little knowledge is available regarding
55 mammalian cellular responses to cooling compared to heat shock responses, which have been
56 previously characterized[16].

57 Here, we use complementary unbiased strategies to gain clues into the MHR upstream of
58 *SP1*. Specifically, we use a novel *SP1* mild hypothermia indicator (MHI) containing the *SP1* promoter
59 and the MCRE enhancer (SP1+MCRE-MHI) to perform compound screening of 1953 FDA-approved
60 agents. We have successfully identified and validated that the drug Entacapone activates the
61 endogenous MHR at the transcriptional level, which indicates that it is possible to manipulate the
62 response without exposure to hypothermia. To identify additional regulators, we have performed a
63 genome-wide CRISPR-Cas9 forward mutagenesis screen[17–19], reading out *SP1*-promoter activity using
64 the SP1-MHI. Our study has yielded multiple candidate regulators and compounds that may regulate

65 the MHR. We focus on one of these regulators, *SMYD5*, a histone methyltransferase, and
66 demonstrate that the presence of SMYD5 is temperature dependent and that several other SMYD5-
67 bound genes show significant differential expression upon mild hypothermia exposure. Our insights
68 elucidate how an external cue (mild hypothermia) specifically mediates its effects on the mammalian
69 genome through the actions of the epigenetic machinery and this paves the way towards the
70 development of a novel therapeutic means to treat neonatal hypoxic-ischemic brain injury, a major
71 cause of mortality and morbidity in otherwise healthy newborns[20], without exposure to TTM.

72 **Results**

73 Mild hypothermia indicators show increased fluorescence at mild hypothermia (32°C).

74 Core temperature (euthermia) is kept at a very tight range in humans (36.5-37.8°C)[1,21] and by
75 definition, mild hypothermia involves temperature ranges from 32-36°C (**Figure S1**, bold). To directly
76 visualize the promoter activity of three genes previously shown[8,15] to respond to mild hypothermia
77 (*CIRBP*, *RBM3*, *SP1*), we have made eight distinct MHIs (**Supplementary Table 1** and **Supplementary**
78 **File 1**) all of which have promoter and/or MCRE sequences, driving the expression of either GFP or
79 mCherry (**Figure 1A**). When transfected into HEK293 cells, the MHIs demonstrate increased
80 fluorescence at 32°C compared to 37°C (**Figure 1B–1C)**. These findings are mirrored by increased
81 endogenous SP1 levels in a Western blot from cells collected after 16 hours (h) at 32°C (**Figure 1D**).
82 We assessed the temporal dynamics of promoter activity using flow cytometry analysis of the three
83 indicators and observed a maximal increase in fluorescence of SP1-MHI between 6-8 h after a
84 temperature shift to 32°C ($P<0.05$, **Figure 1E**). This finding was supported by continuous monitoring
85 of fluorescence from an Incucyte S3 (Sartorius) where again maximal intensity was reached within 6-
86 8 h, with SP1-MHI, rising fastest, followed by RBM3-MHI, and then CIRBP-MHI (**Figure S2A-S2C**).
87 Indicators were also transiently transfected into HEK293 cells and then exposed to five distinct
88 temperatures (26°C, 29°C, 32°C, 37°C, and 40°C), for 16 h followed by flow cytometry **(Figure 1F-1H;**
89 **Figure S2D-S2E**). Consistent with previous literature[8,15] and our own validation in HEK293 cells
90 (**Figure 1B-D**), indicators representing all three genes (*SP1*, *CIRBP*, *RBM3)* had significantly ($P<0.0001$)
91 increased fluorescence at 32°C compared to 37°C/40°C (**Figure 1F-1H**) and the response was
92 uniformly strongest at 32°C (**Figure 1F-1H**). At the same time, the SP1- and CIRBP-MHIs do not show
93 increased activity at lower (26°C, 29°C, **Figure S2D-S2E**) or higher (40°C) temperatures (**Figure 1F-1G**),
94 supporting the notion that our MHIs specifically reflect the MHR and are not activated by general cell
95 stress (i.e., moderate hypo- or hyperthermia). These data suggest that all three genes are regulated
96 at the transcriptional level and the time-lag in the response upon hypothermia is measured in hours
97 rather than minutes, indicating that there must be additional regulators operating upstream of these
98 genes. Some would argue that storing cells on ice (i.e., during fluorescent activating cell sorting

(FACS)) could possibly lower the temperature of cells to the hypothermic range and activate the MHR, but we found that even prolonged storage on ice (8 h) in a room at room temperature was unable to activate the MHI (**Figure S3**), ensuring that storage on ice during the study could not act as a potential confounder.

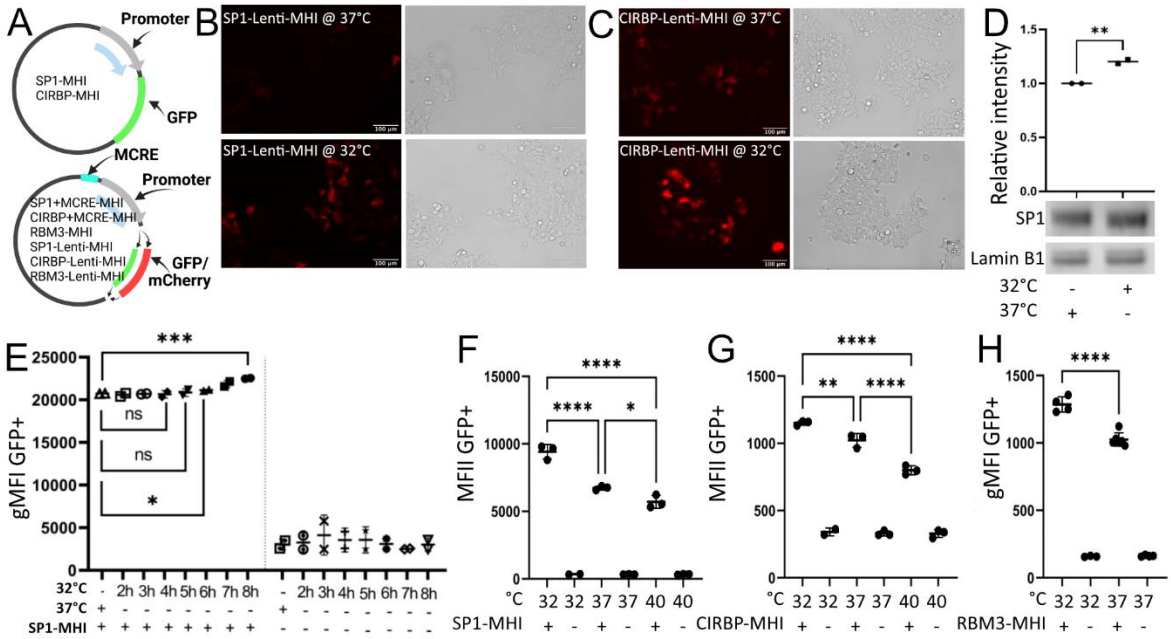

Figure 1. MHIs based on all three genes (*SP1*, *CIRBP*, *RBM3*) show the strongest effect at 32°C. (A) A schematic of MHI structures. (B-C) Representative images of SP1-Lenti-MHIs and CIRBP-Lenti-MHI, respectively, at 37°C and 32°C as visualized by fluorescent microscope. (D) Western blot quantification and a representative figure demonstrating increased SP1 after 16 h at 32°C compared to 37°C. Shown are data points, each data point is a biological replicate and the mean is depicted. Significance levels were calculated with an unpaired two-tailed t-test in GraphPad Prism. (E) Geometric mean fluorescence (gMFI, flow cytometry) after varying lengths of hypothermia exposure for SP1-MHI. Shown are data points, each data point is a technical replicate, mean and SD where applicable. Significance levels were calculated with an unpaired one-tailed t-test in GraphPad Prism. (F-G) Mean fluorescence (MFI, flow cytometry) of SP1-MHI and CIRBP-MHI, respectively, (16 h at 32°C, 37°C, 40°C). Shown are data points, each point is a technical replicate, mean and SD where applicable. Significance levels were calculated in GraphPad Prism with Šidák's multiple comparison test. (H) gMFI of RBM3-MHI (16 h at 32°C and 37°C). Significance levels were calculated with an unpaired one-tailed t-test in GraphPad Prism otherwise data shown as in (G-H). * = P<0.05, ** = P<0.01, *** = P<0.001, **** = P<0.0001.

Activation of the MHR at 32°C is uniformly seen in cells of diverse origins.

In addition to HEK293 cells, which have been widely used in prior MHR studies[11,15,22], we sought to verify that our novel MHIs also work in diverse cellular systems. We transiently transfected three individual MHIs (SP1-, RBM3-, SP1+MCRE-MHI) into seven distinct cell lines: (HEK293WT,

123 HEK293T, HCT-116, HeLa, Jurkat, K562, and SK-N-SH), representing diverse cellular origins including
124 embryonic kidney, colon, cervix, T lymphocytes, lymphoblasts, and neurons, respectively. After
125 exposing these cells to 26°C, 29°C, 32°C, 37°C, and 40°C for 16 h and quantifying the fluorescence by
126 flow cytometry, we observed highest fluorescence at 32°C independent of cellular origin (**Figure S4**)
127 and no effect for moderate hypothermia (26-29°C, **Figure S5**, and **Figure S2D-S2E**) with the exception
128 of SK-N-SH and K562 cell lines (**Figure S5D-S5E**). The strongest activation of MHI at 32°C was
129 detected in the cell-types previously described to have neurological characteristics (HEK293 and SK-
130 N-SH)[23–25] and these were also the cell lines that showed significant activation of all three MHIs at
131 32°C (**Figure 1F-1H**, and **Figure S4**). This is consistent with prior literature showing that the RBM3-
132 MHR response is strongest in young neurons[26]. Since many of the key studies in the field have used
133 HEK293 [11,15,22] and they have neuronal characteristics[23,25] we used this cell line for our screening
134 approaches.

135 Compound screening reveals MHR activators at euthermia.

136 In our search for therapeutic targets for TTM, we sought to identify compounds that could
137 activate the MHR at 37°C as this could yield insights into the involved biochemical pathways. To
138 explore this in an unbiased manner, we performed a systematic library drug screen (1953 FDA-
139 approved inhibitors, **Figure 2A**) using HEK293T cells transfected with the SP1+MCRE-MHI. Cells
140 transfected with SP1+MCRE-MHI were exposed to the drugs (20 µM concentration) and fluorescence
141 was measured after 16, 28, and 40 h of drug exposure (**Figure 2A**). We focused on drugs that increase
142 the MHI fluorescence at least ≥3.75 times at one of the time points (**Supplementary Table 2**). Among
143 these drugs we saw an apparent albeit non-significant enrichment of Tyrosine Kinase Inhibitors (TKI,
144 7/80, $p<0.075$) including Orantinib, Dasatinib (hydrochloride, monohydrate), Poziotinib, Rociletinib,
145 Afatinib, and Lapatinib[27–31]. We validated three from this group (Dasatinib, Orantinib, and Poziotinib)
146 as well as selecting another 5 drugs that showed one of the greatest responses in the screen
147 (Cinacalcet, Entacapone, Erythromycin, Naloxone, and Tamoxifen, **Figure 2B**). For validation of the
148 drug screen HEK293 cells expressing SP1-MHI were individually exposed to each of the 8 compounds
149 (20 µM) for 16 h at either 32°C or 37°C followed by flow cytometry. Two out of the eight (25%),
150 showed significantly ($P<0.001$, $P<0.0001$) increased fluorescence at 37°C (Entacapone, Poziotinib,
151 **Figure 2C-2D**), indicating these two drugs can potentially induce the MHR. Entacapone also had
152 significantly ($P<0.01$) enhanced fluorescence levels at 32°C (**Figure 2C**), suggesting that the effect is
153 additive and thus synergistic to the regular response and thus likely independent of the SP1 target
154 itself. Other compounds did not increase the fluorescence of the SP1-MHI for the dose tested (**Figure**
155 **S6A-S6F**). To exclude the possibility of cell cycle arrest or increased apoptosis[31,32], we evaluated the
156 cell cycle phase in HEK293 cells exposed to Poziotinib and Entacapone, and no apparent signs of cell

cycle arrest were observed for either compound, other than a slight increase in the percentage of total cells in the S phase of the cell cycle after Entacapone exposure (**Figure S6G**). After exposing HEK293 cells to the pro-oxidant agent H_2O_2 in order to induce apoptosis, we could not see any signs of activation of the SP1-MHI (**Figure S6H**), but we observed a significant (P<0.01) increase in fluorescence after only 4 h at 32°C (**Figure S6H**) suggesting that cell stress may potentiate the response. To our surprise, three drugs (Cinacalcet, Dasatinib, and Tamoxifen) showed significantly decreased fluorescence of the SP1-MHI at 32°C during this validation (**Figure S6A**, **S6B**, and **S6F**). To evaluate the endogenous effects on SP1 we carried out Western blotting after 24 h exposure to the compounds at either 32°C or 37°C. For Entacapone (20 µM concentration) we observed a significant increase of SP1 at 37°C (P<0.05, **Figure 2E**). We were unable to test Poziotinib at 20 µM due to low protein yields, therefore, we performed the Western blot at a lower dose (4 µM) and for this dose we only saw a trend towards increased SP1 at 37°C (**Figure 2F**). When we looked at mRNA levels for *SP1*, *CIRBP*, and *RBM3* at 32°C and 37°C after 16 h of Entacapone and Poziotinib exposure (20 µM), we only observed a significant (P<0.01) elevated *RBM3* mRNA levels upon Poziotinib exposure at 37°C (**Figure S7**). This could suggest that the drugs may impact both transcriptional and post-transcriptional levels of key factors of the MHR.

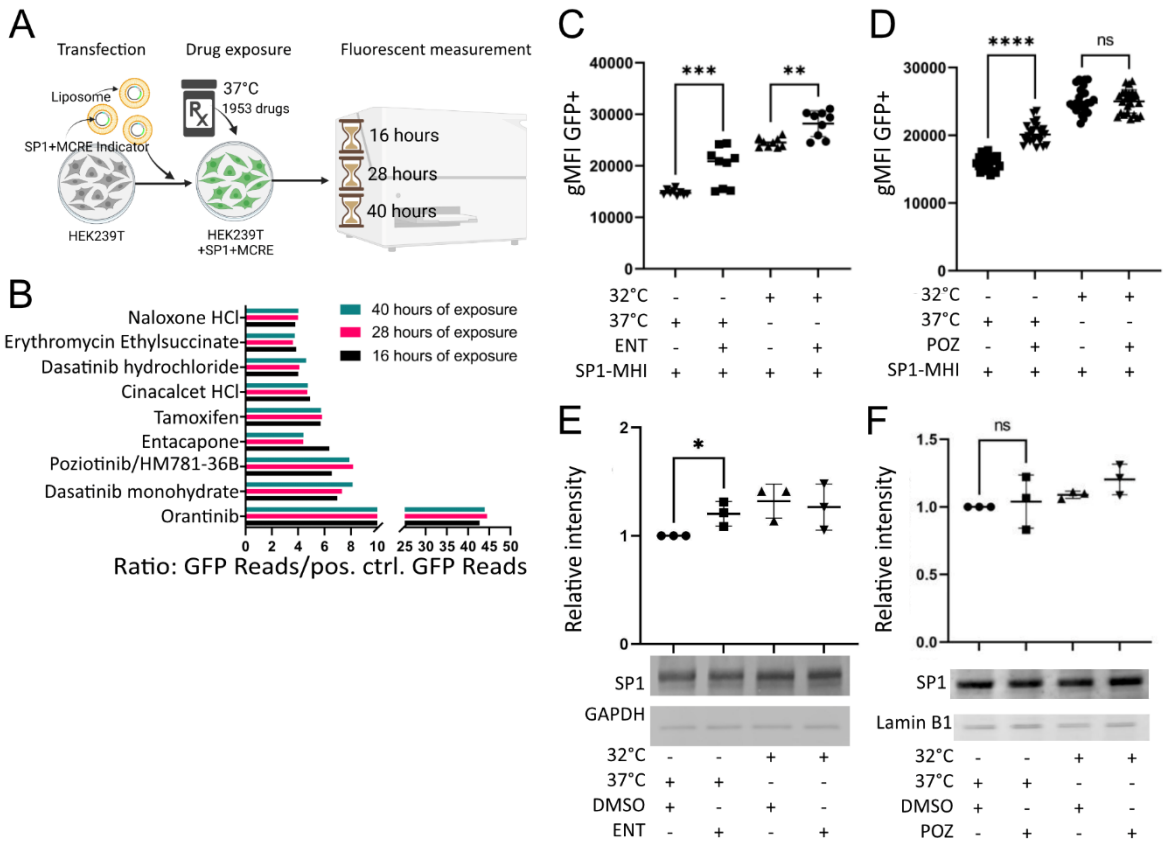

174 **Figure 2. Poziotinib and Entacapone activate the MHR.** (A) A schematic overview of our drug screen
175 in HEK293T cells transfected with SP1+MCRE-MHI. (B) Representative drugs that were found to cause
176 more than ≥3.75 times increase of SP1+MCRE-MHI fluorescence. The entire list is provided in
177 **Supplementary Table 2**. (C-D) gMFI of SP1-MHI as measured by flow cytometry after 16 h of either
178 32°C or 37°C with or without Entacapone (ENT, C, 20 µM) and Poziotinib (POZ, D, 20 µM) exposure.
179 Shown are data points, each point is a technical replicate, mean and SD where applicable.
180 Significance levels were calculated in GraphPad Prism with Šidák's multiple comparison test. (E-F)
181 Western blot quantification and a representative figure of SP1 after exposure to Entacapone (ENT, E,
182 20 µM) and Poziotinib (POZ, F, 4 µM) or vehicle (DMSO) after 24 h. Shown are data points, each data
183 point is a biological replicate, mean and SD where applicable. Significance levels were calculated with
184 an unpaired one-tailed t-test in GraphPad Prism. * = P<0.05, ** = P<0.01, *** = P<0.001, **** =
185 P<0.0001.

186 CRISPR-Cas9 Knockout Screen with SP1-MHIs reveals candidate regulators.

187 To map regulators of the cooling response (*SP1*) in an unbiased manner, we used an available
188 genome-coverage lentiGuide-Puro pooled sgRNA library[17–19] in combination with our SP1-MHI to
189 uncover transcriptional regulators of *SP1*. We chose to use the SP1-MHI, as our prior data indicate
190 that this gene is regulated at the transcriptional level (**Figure 1**) and is the quickest key MHR gene to
191 achieve maximal response at 32°C (**Figure S2A-S2C**). However, given that it does not reach its
192 maximal response until 6-8h of hypothermia exposure, we hypothesized that there may be unknown
193 regulators of the *SP1* locus that function earlier in the MHR process. We performed the screen on
194 HEK293WT+Cas9 cells expressing SPI-MHI (HEK293WT+Cas9+SP1), transducing the sgRNA library at
195 the rate of 0.3 sgRNA per cell. After puromycin selection and exposure to hypothermia (32°C) for 16
196 h (to activate the MHR), we sorted out the 5% most and least fluorescent cells (**Figure 3A**) to capture
197 repressors and activators of *SP1*, respectively. We saw a consistent shift towards lower fluorescence
198 for the transduced HEK293WT+Cas9+SP1-MHI (green) compared to the positive control (non-
199 transduced HEK293WT+Cas9+SP1-MHI, grey, **Figure 3B**). The observation of such a large fluorescent
200 shift of cells (less SP1-MHI fluorescence) at hypothermia suggests the involvement of many sgRNAs,
201 and thus there are likely many genes that are upstream of *SP1*. Furthermore, this suggests that the
202 majority are activators rather than repressors of the SP1 arm of the MHR. We amplified guides for
203 each sorted group as well as the negative control (transduced HEK293WT+Cas9) and performed deep
204 next-generation sequencing of their distribution from sorted and un-sorted fractions (negative
205 control). To identify guides enriched in the sorted populations, we used the MaGeCK pipeline[33] to
206 computationally predict genes with enrichment (**Figure 3C-3D**). We decided to cast a wide net and
207 look at all genes that had a -Log10(RRA) score above 2.5 to not miss possible regulators
208 (**Supplementary Table 3**). We excluded 21 genes that were seen in lists for both the high (repressor
209 list) and low (activator list) sorts of transduced HEK293+Cas9+SP1-MHI (**Supplementary Table 4**), as
210 these may be related to proliferation rather than the MHR itself, and a validation of two of these

211 (*RGS21* and *MALT1*) supported that idea (**Figure S8**). We were left with a list of 495 genes for the
212 SP1-repressors and 61 for SP1-activators – a clear overrepresentation of repressors to activators
213 (**Supplementary Table 3**). Of note, there were two microRNAs on the top list of SP1-repressors and
214 activators (*hsa-mir-4314* and *hsa-mir-6739*) and both are predicted to target SP1 (mirdb.org).

215 Since the ERBB2/HER2 signaling is known to regulate SP1 binding through phosphorylation[34],
216 and is the target of tyrosine kinases inhibitors such as Poziotinib (**Figure S9A**), we looked through
217 both lists and noted that ERK was found on the SP1-repressor list (**Figure S9A**). On the Ingenuity
218 Qiagen ERBB2 Pathway there are 22 genes upstream of *SP1*, and among those, 3 were found on the
219 SP1-repressor list (*RAS*, *ERK*, *STAT5*, P<0.02). We also used the Molecular Signature Database
220 (MSigDB) to establish likely pathways from genes that had a -Log10(RRA) score above 0.5 from each
221 screen (**Figure S9B-S9C**) and observed one shared pathway (Pentose Phosphate Pathway (3P)). Of
222 interest there were two categories in the SP1-activator analysis that implicate cytosolic calcium
223 regulation; calcium influx has been previously shown to be an early event in cells exposed to
224 hypothermic stimuli[35]. As we were particularly interested in a possible transcriptional regulator of
225 *SP1*, we annotated our lists and identified 50 (10%) on the SP1-repressor list and 4 (6%) on the SP1-
226 activator list (**Figure 3E**) as transcriptional regulators. Of these, ten (*GATAD2*, *POU4F3*, *ZNF71*, *KAT5*,
227 *ZNF260*, *ANKZF1*, *SMYD5*, *DMRT1*, *TAF13*, *NKX6-2*) had a -Log10(RRA) score above 3,5 in either the
228 repressor or activator screen (**Figure 3F**). For a gene from our list to act as a direct repressor or
229 activator for *SP1* we reasoned that regulators from the repressor list should have a known function
230 as repressors and genes from the activator list should have known activating functions. Four genes
231 from the list appeared to have opposing functions (*KAT5*, *ZNF260*, *NKX6-2, ANKZF1*, **Figure 3F**, not
232 bold)[36–39] leaving six genes (**Figure 3F**, bold)[40–46] on our list. Histone modification has previously been
233 known to dictate temperature-dependent sex determination in reptiles[47] and vernalization in
234 plants[48], and one of these six targets (*SMYD5*) is a histone methyltransferase, known to catalyze
235 H4K20, H3K9, and H3K36 trimethylation[44,45]. Interestingly, SMYD5 is a likely interactor with KDM6B in
236 fish[49] and KDM6B mediates the previously described epigenetic temperature dependent sex
237 determination switch in reptiles[47]. Also, like CIRBP and RBM3, SMYD5 is a known resident of stress
238 granules[50]. Since SMYD5 histone tail modifications are known and their levels can be measured at
239 *SP1* and other targets we argued that this might be useful for validation purposes. Thus, we decided
240 to further focus our efforts on *SMYD5*.

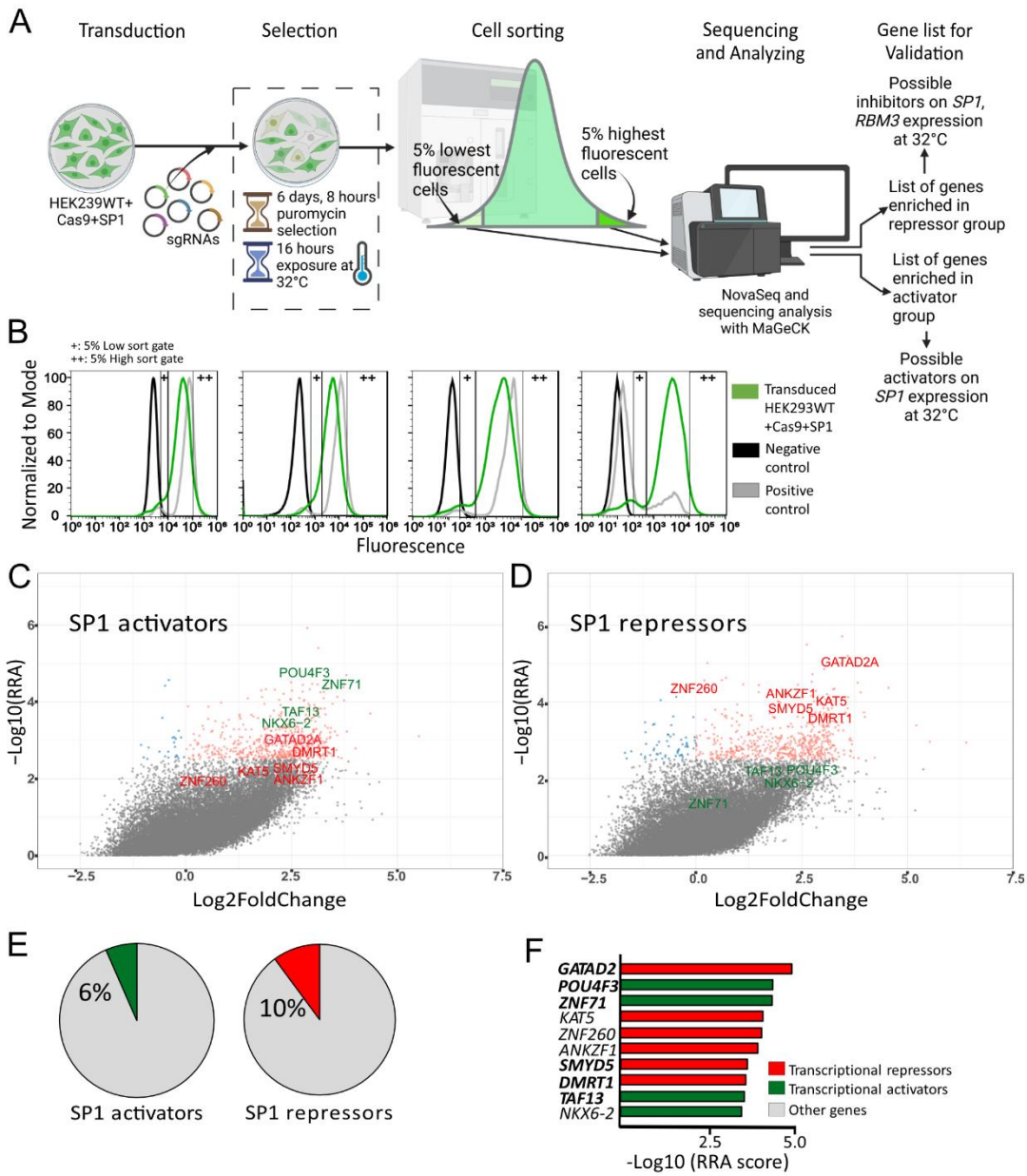

Figure 3. Genome wide CRISPR-Cas9 knockout screen on SP1-MHI reveals multiple potential inhibitors and activators of the MHR. (A) Overview of the genome-wide CRISPR-Cas9 Knockout approach for the HEK293WT+Cas9+SP1 cell line. (B) Fluorescence and sort gates of 4 replicates of transduced HEK293WT+Cas9+SP1 cells (green), negative control (HEK293WT, black) and positive control (HEK293WT+Cas9+SP1, grey). (C-D) Genes marked with their name in red are transcription regulators that have a -Log10(RRA) score >3.5 and have a repressive functions and genes marked with their name in green are transcription regulators that have an activating functions and a -Log10(RRA) score >3.5. Colored dots represent genes that have a -Log10(RRA) score >2.5, where the orange dots indicate genes that have a positive log fold change (LFC) and the blue dots indicate genes that have a negative LFC, from either the SP1 activator (C) or repressor (D) screen. (E) A summary of transcriptional regulators from our screens, activators (green) on left, repressors (red) on right. (F) A summary of top 10 transcriptional regulators ranked by their -Log10(RRA score). Genes in bold are

254 known in the literature to act in the same way as the screen results indicated, that is either as a
255 direct repressor (red) or activator (green).

256 SMYD5 is a direct repressor of *SP1*.

257 To further explore the role of SMYD5, we took advantage of a newly published dataset[44]
258 from a CUT&TAG assay in mouse Embryonic Stem Cells (mES) with an overexpressed SMYD5-Flag
259 plasmid. Upon re-analysis of these data, we noticed that SMYD5 has strong peaks at the promoters
260 of both *Sp1* (130K) and *Cirbp (70K),* but not *Rbm3* (**Figure 4A**). These peaks occur at evolutionarily
261 conserved sites and overlap with CpG islands (**Figure 4A**). We took advantage of an RNASeq dataset
262 on *Smyd5* knockout (KO) mESC from the same study[44] and reanalyzed it which yielded approximately
263 equal amounts of upregulated and downregulated genes among SMYD5 bound loci (**Figure 4B**)
264 supporting prior reports that histone marks deposited by SMYD5 can either repress or activate[44,45].
265 When looking at the three loci (*Sp1*, *Cirbp*, *Rbm3*), we found that *Smyd5*-KO yielded increased
266 expression of *Sp1* but not *Cirbp* or *Rbm3* (**Figure 4C**) suggesting a direct role for SMYD5 as an *Sp1*
267 repressor in a murine system. In this dataset, *Cirbp* showed lower expression compared to *Sp1* and
268 *Rbm3* (**Figure S10**) which may impede interpretation. In order to validate these findings in our own
269 system we decided to knockdown *SMYD5* with siRNA in HEK293WT+Cas9+SP1 cell lines, we observed
270 an increased fluorescence of SP1-MHI at 32°C and 37°C (**Figure 4D**). *SMYD5*-KO with a guide RNA
271 (gRNA) and Cas9 significantly decreased amounts of *SMYD5* mRNA expression by qRT-PCR (**Figure 4E**)
272 and SMYD5 protein levels by Western blot (**Figure 4G**), which are rescued upon overexpression of a
273 gRNA-resistant Flag-SMYD5 plasmid (Flag-SMYD5 sgRNAres plasmid [labelled SMYD5sgRNA#6res],
274 **Figure 4E and 4G**). The same experiment revealed de-repression of the *SP1* transcript in KO cells by
275 RT-qPCR, with repression restored in rescued cells (**Figure 4F**). Furthermore, we observed a
276 significant increase of SP1 and CIRBP, but not RBM3 following *SMYD5*-KO at 37°C using Western blot
277 of the endogenous loci (**Figure 4H-4J**).

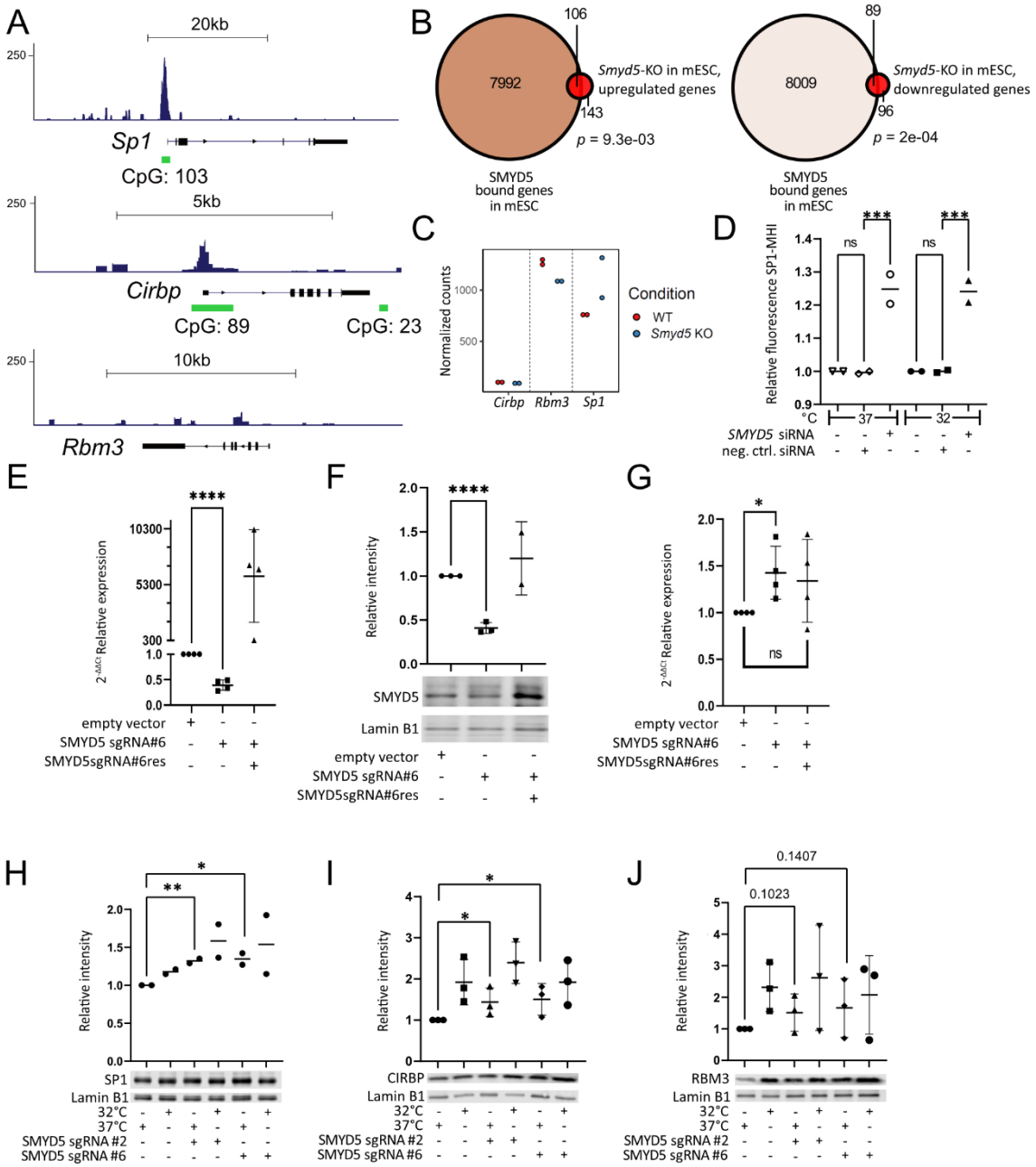

Figure 4. SMYD5 is a repressor of SP1 at 37°C. (A) Overexpressed FLAG-tagged SMYD5 in mESc binds at promoters of *SP1* and *CIRBP* but not of *RBM3*. (B) Venn graph showing both up- and down-regulated SMYD5-bound genes in an RNASeq of *Smyd5*-KO cells. Statistical analysis was done with GeneOverlap package in R using Fisher's Exact test. (C) *Smyd5*-KO leads to increased expression of *SP1* but not *RBM3* or *CIRBP* in mESCs. (D) *SMYD5* knockdown by siRNA yields higher levels of fluorescence of SP1-MHI at 32°C and 37°C compared to empty vector control. Shown are data points, each data point is a biological replicate that has been normalized against the same non-transfected HEK293WT+Cas9+SP1-MHI cell line and a mean of data points. Significance levels were calculated with Šidák's multiple comparison test in GraphPad Prism. (E) Relative expression of *SMYD5* compared to GAPDH from *SMYD5*-KO cells, measured by RT-qPCR at 37°C, with or without rescue with Flag-SMYD5 sgRNAres plasmid (labelled SMYD5 sgRNA#6res) which demonstrates that SMYD5-KO was

290 successful. Shown are data points, each data point is a biological replicate, mean and SD where
291 applicable. Significance levels were calculated with an unpaired one-tailed t-test in GraphPad Prism.
292 (F) Western blot quantification and representative figure using antibodies against SMYD5 and Lamin
293 B in a *SMYD5*-KO cell line with and without rescue with Flag-SMYD5 sgRNAres plasmid (labelled
294 SMYD5 sgRNA#6res) shows that *SMYD5*-KO was successful on protein level at 37°C. Data shown as in
295 (E). (G) Relative expression of *SP1* compared to GAPDH from *SMYD5*-KO cells, measured by RT-qPCR
296 at 37°C, with or without rescue with Flag-SMYD5 sgRNAres plasmid (labelled SMYD5 sgRNA#6res).
297 *SMYD5*-KO leads to increased expression of *SP1* showing that effect is secondary to targeting of
298 *SMYD5* but not something else. Data shown as in (E). (H-J) Western blot quantification and a
299 representative figure using antibodies against SP1, CIRBP and RBM3, respectively, in *SMYD5*-KO cells.
300 Shown are data points, each data point is a biological replicate, mean and SD where applicable.
301 Significance levels were calculated with an unpaired one-tailed t-test in GraphPad Prism. * = P<0.05,
302 ** = P<0.01, *** = P<0.001, **** = P<0.0001.

303 SMYD5 shows temperature dependent expression *in vitro* and *in vivo.*

304 To test whether SMYD5 shows differential expression levels at 37°C and 32°C, we performed
305 a Western blot on HEK293 for SMYD5 using a custom antibody against SMYD5[51] that showed
306 significantly decreased SMYD5 at 32°C (P<0.01, **Figure 5A**). This difference was not observed at the
307 transcriptional level (**Figure 5B**) indicating that SMYD5, is primarily regulated post-transcriptionally.
308 To validate this further we performed immunofluorescence staining where we observe nuclear and
309 cytoplasmic staining of SMYD5 at 37°C (SMYD5; white or green, DAPI; purple, **Figure 5Ca**) and at 32°C
310 (**Figure 5Cb**). The expression of SMYD5 was significantly (p<0.05) decreased at 32°C compared to
311 37°C (**Figure 5C-5D** and **Figure S11A**). We validated this by using an anti-FLAG antibody in cells with
312 overexpression of SMYD5-FLAG[44], which yielded a similar result (**Figure S11B**). We observed a non-
313 significant difference in nuclear to whole cell SMYD5 mean intensity ratio at the two temperatures
314 (**Figure 5E**), suggesting that the levels are equally affected in both compartments at 32°C. Finally, we
315 show that the brains of mice cooled in a standard regimen used to treat neonatal hypoxic-ischemia[52]
316 show a similar temperature-dependent nuclear decrease in SMYD5 after 6 h of cooling, both in
317 neurons of the dentate gyrus (DG) region of the hippocampus (**Figure 5Fa-d**) and cortical neurons
318 (**Figure 5Fe-h**), indicating a SMYD5-dependent impact on the MHR during standard TTM regimen in
319 mice.

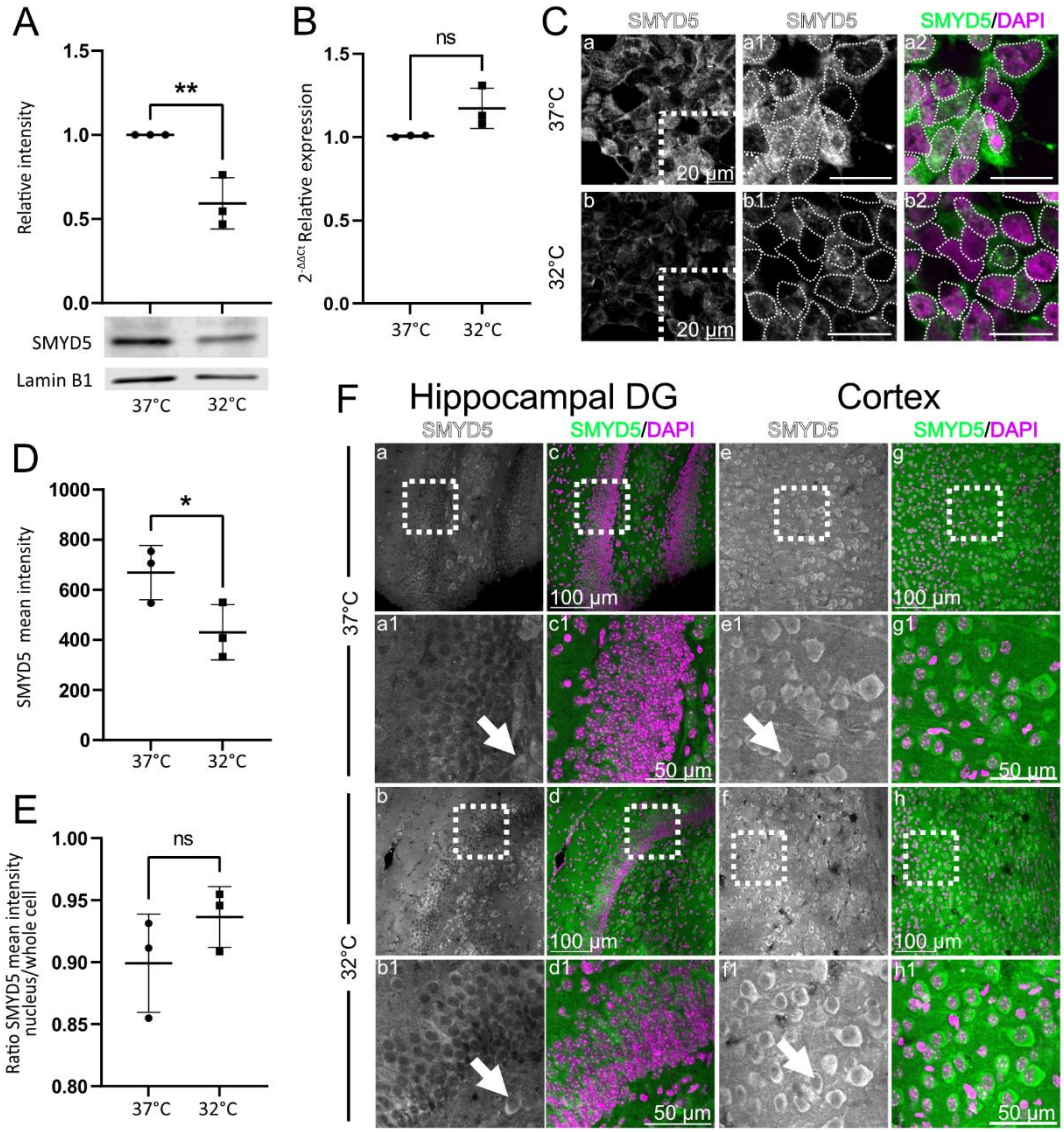

Figure 5. SMYD5 is depleted at 32°C *in vitro* and *in vivo*. (A) Western blot quantification and a representative figure with a SMYD5 antibody at 37°C and 32°C after 6 h incubation. Significance levels calculated with an unpaired two-tailed t-test in GraphPad Prism. Shown are data points, each data point is a biological replicate, SD and mean are depicted where applicable. (B) qRT-PCR results for SMYD5 expression at 37°C and 32°C after 6 h incubation. Significance levels calculated with an unpaired one-tailed t-test in GraphPad Prism, otherwise data shown as in (A). (C) Intensity of endogenous SMYD5 at 37°C (top, a) and 32°C (bottom, b) after 6 h incubation. Nuclei are marked with a dotted line. (D) Cellular SMYD5 mean intensity levels. Data shown as in (B). (E) SMYD5 nuclear to whole cell mean intensity ratio. Data shown as in (B). (F) SMYD5 staining in brain slices of mice kept at euthermia (37°C) compared to mice that had been cooled down to 32°C for 6 h, mouse model of TTM. Brain slices are from the hippocampal DG (a-d) and cortical (e-h) region. * = P<0.05, ** = P<0.01, *** = P<0.001, **** = P<0.0001.

Epigenetic and transcriptional consequences of temperature-dependent changes in SMYD5.

335 As SMYD5 is decreased at 32°C and SMYD5-binding peaks overlap a CpG-island (**Figure 4A**),
336 we performed DNA methylation (DNAm) analysis using the 850 K EPIC Illumina array and observed
337 limited DNAm at 16/18 sites and no differential DNAm at *SP1*, *CIRBP* or *RBM3* promoters at 32°C for
338 6 h compared to 37°C at CpGs spanning each of the gene regions (**Figure S12** and **Supplementary**
339 **Table 5**). However, there was differential DNAm at other CpGs loci after 6 h exposure at 32°C
340 (**Supplementary Table 6**) supporting the idea that the MHR is regulated by the epigenetic machinery.
341 To further explore the epigenetic consequences of differential SMYD5 availability at 37°C versus
342 32°C, we performed CUT&RUN using antibodies against H3K36me3, H4K20me3, H3K9me3,
343 H3K4me3, H3K27me3, SMYD5 and H3 (control) in HEK293 cells and human neural progenitor cells
344 (NPCs). We chose H3K36me3, H4K20me3, and H3K9me3 since these modifications have been
345 previously shown to be deposited by SMYD5[44,45]. We also chose to look at H3K4me3 and H3K27me3
346 as these are general open and closed chromatin modifications that are also known to change during
347 vernalization in plants[53]. We saw less H3K36me3 over *SP1* at 32°C compared to 37°C in NPCs (**Figure**
348 **6A**) and HEK293 cells (**Figure S13A**) as well as decreased global SMYD5 binding (**Figure 6B**), all
349 consistent with lower SMYD5 amounts at 32°C (**Figure 5**). We further observed a global deficiency of
350 H3K36me3 at 32°C compared to 37°C seen in both HEK293 cells (**Figure 6C**) and NPCs (**Figure S13B**)
351 albeit more prominent in NPCs indicating that this modification is used to regulate additional genes
352 perhaps through SMYD5 but levels of SMYD5 mirror this effect (**Figure 6B** and **Figure 5**). We also
353 observed a global H3K4me3 deficiency at 32°C compared to 37°C (**Figure 6D**), although there were
354 also 1288 genes that had a unique H3K4me3 modification at 32°C which was not seen at 37°C
355 (**Supplementary Table 8**). For H3K9me3 we saw a deficiency of histone modification marks upstream
356 of gene bodies in NPCs (**Figure 6E**). We did not observe a difference for other histone modifications
357 when comparing 32°C and 37°C in NPCs (**Figure S13C-S13D**). CUT&RUN for H3K36me3 also revealed
358 several significantly differentially modified genes at 32°C when compared to 37°C (**Figure 6F**, **Figure**
359 **S13E**, **Figure S14**, and **Supplementary Table 7**) including a number of epigenetic regulators, such as
360 *BAZ2A* and *SETD1B* (**Figure 6F**, **Figure S14A**, and **Figure S14E**). To identify additional genes regulated
361 by SMYD5 and temperature, we performed an RNASeq in mouse NPCs (mNPCs) at the two
362 temperatures. This yielded 2890 differentially expressed genes (DEGS) that were upregulated and
363 3133 DEGS that were downregulated at 32°C compared to 37°C. Interestingly, when we overlap
364 upregulated DEGS in mNPCs at 32°C with SMYD5-bound and repressed genes (*Smyd5*-KO
365 upregulated) at 37°C in mESCs we observe a statistically significant overlap of 26 genes (P=5.4e-04,
366 **Figure 6G**). Similarly, when we overlap down-regulated DEGS in mNPCs at 32°C with SMYD5-bound
367 and upregulated genes (*Smyd5*-KO downregulated) at 37°C in mESC we also observe an overlap of 19
368 genes (P=0.029, **Figure 6H**). This suggests that SMYD5 regulates additional genes in a similar manner
369 to *SP1* (as a repressor at euthermia) as well as regulating some in an inverse manner (normally as an

370 activator at euthermia) in murine models. This includes several genes upregulated at 32°C with a
371 theoretically appealing role for hypothermia responses such as *Klf15* (role in brown adipose tissue
372 metabolism)[54] and *Thrap3* (role in thyroid metabolism and adipocyte differentiation)[55,56]. Among the
373 genes normally upregulated at 37°C but downregulated at 32°C, *Bnip3L*, a pro-apoptotic gene[57] is of
374 particular interest given the previously observed cytoprotective role of mild hypotherma[9–13]. We
375 provide the entire list of 45 SMYD5-temperature dependent genes in **Table 1.** When we looked more
376 closely at the list of genes that had unique H3K4me3 modification in NPCs at 32°C and overlapped
377 those genes with human orthologs of upregulated DEGS in mNPCs at 32°C we saw a significant
378 overlap of 169 genes (P=2.4e-03, **Figure 6J,** and **Supplementary Table 9**). Only 6 genes are bound by
379 SMYD5 and upregulated with *Smyd5*-KO at 37°C in mESCs as well as upregulated at 32°C in mNPCs
380 (**Table 1**) and have a unique H3K4me3 peak at 32°C in NPCs (**Supplementary Table 8**). Interestingly
381 *Asxl1,* a member of the Polycomb family[58] a family which is known to take part in vernalization in
382 plants[48], is among these 6 genes. This indicates that there may be additional epigenetic MHR-
383 responses that are independent of SMYD5. Finally, we demonstrate that on average these 45 genes,
384 regulated by SMYD5, have lower H3K36me3 modifications at 32°C versus 37°C at their gene bodies as
385 well as fewer modifications over the 3'-UTR region at 32°C in NPCs and HEK293 cells (**Figure S13F-**
386 **S13G**). In addition, these genes also show a different H3K4me3 and H3K9me3 modification pattern at
387 32°C and 37°C in NPCs when looking at their 3'- and 5'-UTR regions (**Figure S13H-S13J**).

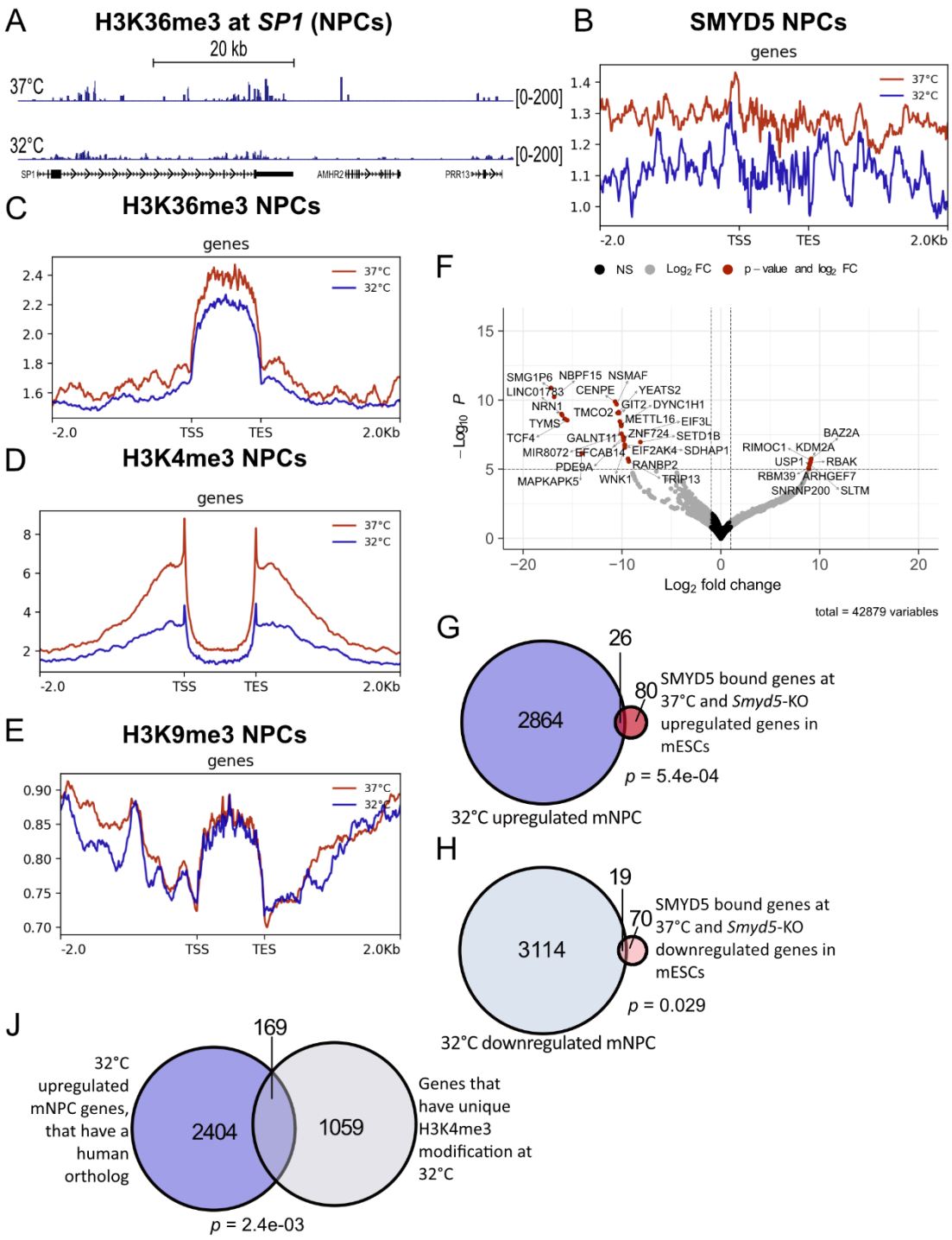

Figure 6. SMYD5 is a novel epigenetic gatekeeper of the MHR. (A) Decreased H3K36me3 is observed at the *SP1* promoter and gene body at 32°C compared to 37°C. (B) SMYD5 chromatin binding is globally decreased (all genes) at 32°C compared to 37°C. (C) There is a global deficiency of H3K36me3 at 32°C compared to 37°C. (D) There is a global H3K4me3 deficiency at 32°C compared to 37°C. (E) Upstream of gene bodies there is a global H3K9me3 deficiency at 32°C compared to 37°C. (F) At the gene-specific levels there are a number of genes, that have significantly altered H3K36me3 at 32°C compared to 37°C in NPCs. Red circles indicate genes that have Log_2 fold change over 1 and p-value less than 10^{-6}, gray circles indicate Log_2 fold change over 1 but non-significant p-value ($>10^{-6}$) and black circles indicate non-significant Log_2 fold change and p-values for those genes. (G-H) DEGS from

398 RNASeq in mNPCs at both temperatures show overlap with SMYD5-bound genes that are
399 differentially expressed upon *Smyd5*-KO in mESCs at 37°C. Statistical analysis was done with
400 GeneOverlap package in R using Fisher's Exact test. (J) There is a significant overlap of DEGS and
401 genes that have a unique H3K4me3 modification at 32°C. Statistical analysis as in (G-H).

402

SMYD5-repressed genes ↑ at 32°C (SMYD5 represses at 37°C)

Gene	Function	Role
Mybl2	Transcription factor	Cell-cycle control
Klf15	Transcription factor	Brown-tissue metabolism
Thrap3	Transcriptional co-activator	Thyroid hormone receptor binding
Tex15	DNA repair protein	Role in testicular meiosis
Ewsr1	RNA binding	Role in Ewing sarcoma
Tfcp2l1	Transcription factor	Pluripotency in stem cells
Amotl2	Angiostatin binding factor	Role in angiogenesis
Phf20	Methyl-lysine-binding protein	Histone modification
Cd24a	Sialoglycoprotein	Cell differentiation
Nt5e	Nucleotidase	Nucleotides metabolism
Neo1	Cell surface receptor	Immunoglobulin superfamily
Gabbr1	GABA receptor	Inhibitory neurotransmitter
Asxl1	Chromatin binding protein	Polycomb family member
Tulp4	Tubby Superfamily Protein	Ubiquitination function
Pkn1	Serine/threonine-protein kinase	Protein kinase C superfamily
Hnrnpul1	RNA-binding protein	hnRNP family
Mier1	Transcriptional regulator	Mesoderm induction early response
Fam21	WASH complex member	Endosomal protein sorting
Trip12	E3 ubiquitin-protein ligase	Ubiquitin regulation and DNA repair
Lamc1	Extracellular matrix glycoprotein	A laminin
Rell1	RELT-like protein	Regulates the p38MAPK cascade
Xrn2	5'-3' exonuclease	Promotes transcription termination
Hspg2	Multidomain proteoglycan	Encodes Perlecan protein
Ctc1	Telomere maintenance protein	Limits telomere degradation
Stag1	Component of cohesin complex	Role in cohesion of sister chromatids
Ass1	Enzyme	Role in urea cycle

SMYD5-upregulated genes ↓ at 32°C (SMYD5 activates at 37°C)

Gene	Function	Role
Usp28	Ubiquitin Thioesterase	DNA damage checkpoint
Ccnd1	Cyclin D	Cell cycle regulation
Dzip3	Ubiquitin-protein transferase	Spermatogenesis
Rad50	DNA double-strand break repair	Cell cycle regulation
Arglu1	Enables cadherin binding	Mediator complex
Sltm	RNA binding activity	Regulation of transcription
Slc16a3	Solute transporter	Lactic acid and pyruvate transport
Ier5l	Unknown function	Parolog of IER5
Acly	Enzyme	Synthesis of cytosolic acetyl-CoA
Agps	Enzyme	Lipid biosynthesis
Apobec3	Cytidine deaminase	RNA editing

Ivns1abp	Viral binding protein	Response to viral infection
Dus3l	Synthesis of dihydrouridine	RNA editing
Upp1	Uridine phosphorylase	Ribonucleosides dynamics
Ldha	Enzyme	Lactate to Pyruvate conversion
Scd2	Enzyme	Fatty acid biosynthesis
Smarcad1	Chromatin remodeler	Role in heterochromatin formation
Bnip3l	Pro-apoptotic protein	Induces apoptosis
Esrra	Nuclear receptor	Mitochondrial biogenesis regulator

Table 1: Summary of temperature responsive SMYD5-regulated genes.

403

404 **Discussion**

405 Histone modification has previously been found to help integrate the effects of cold
406 temperature exposure in diverse organisms. For example, in plants, vernalization, the basis of how
407 cold exposure influences the rate of flowering, is mediated through a Trithorax-Polycomb switch[48]. In
408 some reptiles, sex determination is achieved through a temperature dependent mechanism and for
409 one such, the red eared slider turtle (*Trachemys Scripta Elegans*), this regulation acts through a
410 histone methylation switch[47]. To uncover regulators of the mammalian MHR we used our novel MHIs
411 to identify an FDA-approved drug, Entacapone, that can induce the SP1-mild hypothermia response
412 as well as conducting a forward CRISPR-Cas9 mutagenesis screen resulting in the identification of
413 *SMYD5* as a repressor of the MHR at euthermia. Such insights can be useful to expand the
414 mechanistic understanding of the MHR, but our data also provide both a feasible current strategy
415 (Entacapone) as well as a future therapeutic target (SMYD5) for efforts to activate the MHR without
416 cooling in patients at risk of neurological sequela after catastrophic events. Finally, a detailed
417 understanding of the mammalian MHR is important to understand how temperature can
418 systematically bias results in biology and medicine. One such example involves the process of
419 harvesting tissue from human cadavers but uniformly these are kept at a low temperature which
420 may activate the mild hypothermia response in the cells being harvested. Similarly, countless
421 researchers store samples at room temperature between experimental steps which in some
422 scenarios may activate the MHR. This contrasts with storage on ice but in our own hands that does
423 not appear to activate the MHR. Such data may be of use to a large number of scientists.

424 Our current MHIs, a novel tool for the MHR community, allow for some temporal dissection,
425 yet they all currently harbor stable fluorescent protein, which may capture average responses over
426 time rather than dynamic difference, but the latter can be detected by real time qPCR. Thus, our
427 current MHIs may be the most useful to map the start of the response (as we have done in **Figure 1**).
428 However, in future work, we hope to create unstable fluorescent molecules that break down quickly

429 to help us map the kinetics of different parts of the response, for example, how quickly the response
430 is resolved (i.e., termination).

431 Although our drug screen and validation may have limitations (only three timepoints, single
432 dose), we observe an overrepresentation of TKIs. The reason why some TKIs as well as other drugs
433 did not validate could be that the drug screen was performed using an MHI containing the MCRE (to
434 increase signal) but validation was performed on an MHI lacking the MCRE (the endogenous situation
435 in mammals[15]). Of the TKIs we have further shown that Poziotinib, a known pan-HER inhibitor[29], was
436 able to increase *RBM3* mRNA but not *SP1* or *CIRBP* mRNA (**Figure S7**) or SP1 (**Figure 2F**) at 37°C with
437 the doses tested. The lack of increased SP1 quantified by Western blot could be caused by the
438 relatively low (4 µM) Poziotinib dose compared to what was used for RT-qPCR and flow cytometry
439 (20 µM). Here, we identify and validate Entacapone as a compound that can activate the SP1-MHR at
440 euthermia (**Figure 2E**). Entacapone is a COMT-inhibitor, which is frequently used in the clinic due to
441 its ability to increase dopamine availability by blocking its degradation in synapses[59]. It is interesting
442 that synaptic plasticity is known to be influenced by temperature changes[60]. This suggests that
443 Entacapone may act at the cell membrane since Entacapone is a neurotransmitter breakdown
444 inhibitor (COMT), which acts at the neural synapse. In fact, several candidates (**Figure 3C-3D**) from
445 the CRISPR-Cas9 forward mutagenesis screen appear to operate at the neural synapse or bind to
446 Syntaxin (**Supplementary table 3**) such as *STXBP1* (SP1 repressor) and *TXLNB* (SP1 activator). Both
447 bind to Syntaxin (**www.genecards.org**) and play a role at the neuronal synapse as well as having a
448 role in dopaminergic synaptic transmission[61], and such distal regulation may be worth exploring in
449 future work.

450 Our data support the notion that SP1 and RBM3 may be parts of distinct arms of the
451 mammalian hypothermia response as SMYD5 only regulates *SP1* but not *RBM3*. We interpret the lag
452 in the response (at least 6 hours to signal) and the obvious shift in fluorescence of mutagenized cells
453 to mean that there are likely many genes upstream of the currently tested point of the response
454 (*SP1*). Despite a global shift towards activators, the yield from the enrichment screen yielded more
455 putative *SP1* repressors compared to *SP1* activators. This could be caused by the screen setup as it
456 may be easier in general to find genes that increase fluorescence (repressors) than those that
457 decrease fluorescence (inhibitors), as the latter will overlap with cells that have lost the SP1-MHI for
458 various reasons. Another limitation of our forward screen is that it can only identify cell-autonomous
459 genes and cannot find essential genes. However, it is a starting point, and here we provide 556
460 candidate regulators that can be subsequently validated using our MHIs or other strategies. Of
461 interest, SMYD5 and ERBB2/HER2 (the receptor Poziotinib blocks) have been previously found to
462 functionally interact in a forward mutagenesis screen of genes that play a role in metastatic

463 reactivation and tumor dormancy[62] and additionally, *CIRBP* transcript levels correlate with prognosis
464 in luminal A/B breast cancer, which is influenced by HER2 status[63]. In fact, our SP1-repressor screen
465 revealed several downstream factors of ERBB2 signaling (*RAS*, *ERK*, *STAT5,* **Figure S9A**), indicating
466 that this pathway may be upstream of SMYD5 and worth exploring. Alternatively, SP1 itself may be a
467 target of phosphorylation, and as SP1 is predicted to bind at its own promoter[64] and perhaps both
468 signals are required for full effect.

469 Here, by uncovering *SMYD5* as a negative epigenetic regulator of SP1, a key factor of the
470 mammalian MHR, we provide an example of how histone methylation integrates temperature cues
471 into a fundamental mammalian response. Our present model is that SMYD5 exerts its effects at 37°C
472 to ensure that *SP1*/*CIRBP* are not upregulated without a cold stimulus, however, upon cold stimulus
473 (32°C), SMYD5 is degraded and SMYD5 repression is released, thus activating the MHR. The nuclear
474 SMYD5 repression release upon mild hypothermia could happen because of one of the following:
475 nuclear exclusion of SMYD5, less *SMYD5* mRNA being translated, less protein synthesis, or SMYD5
476 could undergo proteasomal degradation. Per bioGRID, SMYD5 is known to bind to four ubiquitinators
477 (PARK2, UBA52, TRIM25, USP34) so this may be an avenue for further study as such factors often
478 target proteins to the proteasome. Previously, a generalized decrease of protein production upon
479 cold stimulus has been shown to act through AMPK mediated phosphorylation of eEF2K[22], and thus
480 decreased translational efficiency could play a part. However, we are unaware of biological examples
481 of targeted protein degradation in response to mild hypothermia.

482 SMYD5 itself appears to regulate at least 45 other factors that show temperature
483 dependence, 26 in which SMYD5 acts as a repressor (like *SP1*) and another 19 where SMYD5 acts as
484 an activator at euthermia. Some of these genes look like very plausible MHR participants, especially
485 *BNIP3L,*[57] a pro-apoptotic factor that is downregulated with hypothermia and may thus contribute to
486 the neuroprotective/cytoprotective effect of mild hypothermia. There are also genes that play a role
487 in thyroid and adipocyte function (*THRAP3*)[55,56], brown adipose tissue (*KLF15*)[54] and testes
488 (*TEX15*)[65,66], all target tissues of physiological mammalian temperature responses. Coinciding with
489 decreased global H3K4me3 at 32°C, we also observed decreased H3K36me3 at 32°C over the gene
490 *SETD1B* (**Figure 6F** and **S14E**) which encodes an H3K4me3-methyltransferase. In oocytes, *Setd1b*-KO
491 can cause gain or loss of H3K4me3[67]. Accordingly, this could be one potential mechanism underlying
492 H3K4me3 changes at 32°C and warrants further investigation. It is interesting that H3K36me3 has
493 previously been shown to regulate temperature-regulated alternative splicing in plants[68] and in the
494 fungus *Saccharomyces cerevisiae,* H3K4 and H3K36 methyltransferases (Set1 and Set2) regulate
495 alternative polyadenylation[69]. Furthermore, in mice, H3K36me3 has a direct impact on alternative
496 splicing of neurobiological factors in the brain[70]. In mammals' temperature dependent alternative

splicing[71] and alternative splicing of *CIRBP* and *RBM3* have been observed[72–74]. Perhaps alternative splicing or polyadenylation play a role in controlling levels of SP1 or one of the other 45 SMYD5-bound factors elucidated here.

In summary, we have developed and validated novel tools to interrogate the MHR and used them to show, for the first time, that a compound exists that can activate the MHR without cooling. We provide a list of 556 candidate of the MHR pathway and validate *SMYD5* as a temperature-dependent epigenetic gatekeeper of the MHR and, for the first time, show how histone methylation (H3K36me3, H3K9me3, and H3K4me3) changes in mammals with MHR exposure, providing a specific example of how mammalian cells use epigenetics to respond to temperature cues.

Acknowledgements: We thank SCRU lab (UI) for gifting us pMD2.G (Addgene, #12259) and psPAX2 (Addgene, #12260) and H.C. Dietz and D. Valle labs (JHU), for gifting us the HCT-116, SK-N-SH, HeLa, Jurkat and K562 cell lines. We thank Alan Long at the ChemCore facility at JHU and the Pharmacy of Landspitali for support regarding the drug screen and validation. We thank the Immunology department of Landspitali University Hospital for the access and assistance with the FACS sorting. We thank FUNlab at deCODE genetics for the usage of their flow cytometry machines as well as for gifting us the HEK293T cell line. We thank Kári Stefánsson and Ólafur Þ. Magnússon at deCODE Genetics for providing some of the next generation sequencing for this project. We thank Erna Magnúsdóttir for providing pAG-MNase for the CUT&RUN assays as well as guidance with the CUT&RUN experiment and data analysis. This study was supported with funding from the Rannis Technology Development Fund (H.T.B., #2010588), Eimskip University Fund (S.R.), Fulbright Iceland (S.R.), Icelandic Cancer Society Research Fund (H.T.B.), Göngum Saman Research Fund (H.T.B.), Landspitali Research Fund (H.T.B.), Félag Háskólakvenna Research Fund (S.R.). H.T.B. is also supported by funding from Rannís (#217988, #195835, #206806) and the Louma G. Foundation. R.C-V. is supported by Thomas Wilson Foundation and the Johns Hopkins University Pediatric Innovation Grant. R.C-V. and F.J.N. are supported by the NIH R01NS126549, 1R21NS123814, and 1R01 HD110091 and F.J.N. additionally by R01HD074593, U01NS114144. Finally, some images in this manuscript were created with BioRender.com.

Author contributions: H.T.B. and S.R. conceptualized the project. S.R., L.Z., and H.T.B. created and designed the MHIs. S.R., A.T., L.H.A., M.V., K.E.A., and K.J. performed cell culture. S.R., A.T. L.H.A., and M.V. performed flow cytometry experiments. L.Z. and H.T.B. designed the approach to the drug screen. S.R., and H.T.B. designed the approach to the forward mutagenesis assay. S.R. performed the forward mutagenesis assay and drug screen. S.R. and K.J.A. performed the PCR for the NGS. S.R., A.T., and K.J. validated results from drug and mutagenesis screens (Western blots (A.T., K.J.), RT-qPCR (S.R., K.J.) and flow cytometry (S.R., A.T.)). K.J. and K.M. performed IF on cells from culture. K.J. and K.M. performed the confocal imaging and K.M., K.J. S.Th.H., and S.R. did the data analysis. S.R. and M.V. performed siRNA knockdown. R.C-V. and F.J.N. produced the euthermic and hypothermic mouse pups, performed microdissections and perfusions. K.J.A. isolated and cultured mNPCs. M.V. performed cryosectioning and IF on mouse brain slices and M.V. and K.M. performed confocal imaging as well as the analysis of the mouse brain slices. S.R., A.T., and S.Th.H. performed CUT&RUN experiments. K.J.A. did the mNPCs isolation and RNASeq and data analysis. S.R., K.J.A., K.J., A.T.

S.Th.H., and T.R. analyzed data. J.H. provided SMYD5 antibody and K.E.A. provided human NPCs. S.R. and H.T.B. wrote the manuscript and all authors critically reviewed the manuscript. Project administration was carried out by H.T.B, S.R., and K.J.A.

Declaration of interest: H.T.B. is a consultant for Mahzi therapeutics. S.R. and H.T.B. have a European patent application (number 23167505.9).

543 **STAR Methods**

544 **Creation of novel indicators:** We used the PGL4.10 plasmid (Promega, #9PIE665) as the backbone for
545 our CIRBP- and SP1-MHI, where the *luc2* sequence was cut from the plasmid with NcoI (NEB) and
546 XbaI (NEB). Promoter sequence for *CIRBP*[75] was cloned from mouse DNA using *CIRBP* forward primer
547 5'-tcgataggtaccTGGCTTCACAAATGCGCCTCAGT-3' and *CIRBP* reverse primer 3'-
548 cctaaggcagatctGCGAGGGGGAGCGCAAGAGT-5'[75]. Restriction enzymes KpnI (NEB) and BglII (NEB)
549 were used to insert the promoter into the plasmid. Promoter sequence for *SP1*[76] was cloned from
550 human DNA using the forward primer 5'-tcaagtcaggctagcGCAACTTAGTCTCACACGCCTTGG-3' and
551 reverse primer 3'-cagtgctgcctcgagGCTCAAGGGGGTCCTGTCCGG-5'[76]. Restriction enzymes NheI (NEB)
552 and XhoI (NEB) were used to insert the promoter into the plasmid. AcGFP1 was cloned from
553 PT7XbG2-AcGFP1 (Novopro, #V002843) vector using the reverse primer 3'-
554 cggcggagTCTAGAATTACTTGTACAGCTCGTCC-5' and the forward primer 5'-
555 taagccaccATGGTGAGCAAGGGCGAGGAGC-3'. Restriction enzymes NheI (NEB) and XhoI (NEB) were
556 used to insert the acGFP1 into the plasmid. The neomycin selection cassette was cloned from
557 pROSA26-dest plasmid (Addgene, #21189) using the forward primer 5'-
558 CATTATCGTCGACTCTACCGGGTAGGGGAGGCGCTT-3' and reverse primer 3'-
559 CGCCGCCGACGATAGTCAAGCTTCTGATGGAATTAGAACTTGGC-5'. Restriction enzymes SalI (NEB) and
560 PshAI (NEB) were used to insert the neomycin cassette into the plasmid. CIRBP- and SP1-MHI were
561 made with and without MCRE[15]. The MCRE sequence was inserted in 5 repeats in front of the
562 promoter sequences with a linker sequence between. Acc65I (NEB) restriction enzyme was used to
563 insert the MCRE sequence into the CIRBP-MHI and Acc65I (NEB) and SacI (NEB) restriction enzymes
564 were used to insert the MCRE into the SP1-MHI. Sanger Sequencing was used to validate insertion
565 sites, size, and sequence of insertion. The *RBM3* promoter with MCRE enhancer (6 repeats) in front
566 of the promoter was cloned into the multiple cloning site pCMV6-AC-GFP (BlueHeron, #PS100010).
567 We also made lentiviral vectors for *CIRP*, *SP1* and *RBM3* on a pLV-Ex (VectorBuilder) lentiviral vector.
568 The *CIRBP* promoter for the CIRBP-lenti-MHI was designed from the human promoter and the *SP1*
569 promoter was moved upstream of the TSS for the SP1-lenti-MHI but *RBM3* promoter sequence
570 remained unchanged. Included were MCRE (8 repeats for CIRBP-lenti-MHI, five repeats for other),
571 promoter, neomycin selection cassette and a mCherry fluorescent protein behind each promoter
572 sequence. The promoter region, size and backbone plasmid for each indicator is detailed in
573 **Supplementary Table 1** and sequence of each MHI in **Supplementary File 1**. We also observed some
574 variation in absolute levels among individual indicators/experiments, but the pattern was always
575 consistent; given this, we only show data from individual experiments in any figure.

576 **Culture of cell lines:** HEK293 (gifted and DSMZ, CRL-1573, referred to as 293/293WT) cells were
577 cultured in DMEM/F12 with GlutaMAX (Gibco, 10565018) with 10% filtered FBS (Gibco, 10270106)
578 under 5% CO_2. Cells were cultured at 37°C unless otherwise stated, then 37°C served as a control. In
579 addition to HEK293, we used the following cell types HEK293T (gifted, CRL-3216), HCT-116 (gifted,
580 CCL-247), HeLa (gifted, CCL-2), Jurkat (gifted, TIB-152), K562 (gifted, CCL-243), SK-N-SH (gifted, HTB-
581 11). Cells were sub-cultured when they had reached 70-90% confluence and media was changed
582 every other day. Killing curves were used for all cell lines to determine lowest selection concentration
583 for all selection agents. We used culture recommendations from ATCC when possible. We also used
584 human iPS cells (ATCC, ACS-1019) that were used to generate NPCs by neural induction of iPSCs using
585 dual SMAD inhibition and embryoid body generation (StemCell Technologies; 08581, 05832,
586 05838)[77], prior to experiments described here the NPCs were cultured in STEMdiff Neural Progenitor

587 Medium (StemCell Technologies, 05833) on Matrigel (Corning, 354234). As well as murine primary
588 NPCs (see section mNPC isolation for further information).

589 **Transfection of MHI and SMYD5-Flag overexpression plasmid:** HCT116, 293WT, HEK293T, HeLa and
590 SK-N-SH cell lines were transfected with MHI when they had reached 70-90% confluency. We used
591 either Lipofectamine™ 2000 or 3000 (Thermo Fisher Scientific, 11668027, L3000015) according to
592 the manufacturer's protocol. For transfection of K5622 and Jurkat cell lines we used electroporation
593 for transfecting the MHIs into the cell lines. The fluorescence of the indicators was measured via flow
594 cytometry up to 48 h after transfection. We analyzed flow cytometry data with the FlowJo Software,
595 where we gated living cells, single cells, GFP positive cells and measured the fluorescence for that
596 population. For further analysis, we used Excel from Microsoft, GraphPad Prism (v.9) and FlowJo
597 (v.10.8.1). For transfection of SMYD5-Flag overexpression vector[44] we used the same lipofectamine
598 method as described above.

599 **Construction of 293WT+Cas9 and 293WT+Cas9+SP1 cell lines:** We made two cell lines from 293
600 cells, one that expressed Cas9 (lentiCas9-blast, Addgene #52962), referred to as 293WT+Cas9, and
601 another that expressed both Cas9 and SP1-MHI, referred to as 293WT+Cas9+SP1. These cell lines
602 were made by transfecting the plasmids with lipofectamine as described above and selecting stably
603 transfected cells using Blasticidin selection for Cas9 and Neomycin selection for SP1-MHI.

604 **Drug screen:** Briefly, we used Lipofectamine 3000 (Thermo Fisher Scientific, L3000015) to transfect
605 the SP1+MCRE-MHI into the 293T cell line. 24 h after transfection, 30000 cells were plated into each
606 well of a black 96 well plate. 48 h after transfection the cells were exposed to FDA Approved Drug
607 Screening Library (L1300-Z298012) via the High Throughput Screening Services, ChemCore Facilities
608 (Johns Hopkins University). Each drug was exposed in 20 µM final concentration. Total well GFP was
609 read with the CLARIOStar Plus Plate Reader (BMG LABTECH, settings: gain 1500, 470-15 excitation
610 and emission 515-20 at focal height 2.6) 16, 28, and 40 h after exposure of the library. Ratio of
611 increased fluorescence was calculated by dividing GFP reads from positive control (SP1+MCRE-MHI
612 transfected but untreated) at each time point with GFP reads of each whole well exposed to drug at
613 the same timepoint for wells in the same lane. For further analysis, we used Excel from Microsoft and
614 GraphPad Prism (v.9).

615 **Validation of drug screen:** We individually validated 8 compounds in same concentration (20 µM).
616 Here, we exposed the drug for 16 h either at 32 or 37°C, and evaluated by flow cytometry as
617 previously described. In a 96-well plate 20,000 of either 293 or 293+SP1-MHI cells were seeded per
618 well in a total volume of 200 µL of media. After cells had attached to the wells (the morning after),
619 cells were exposed to 20 µM of each drug, controls were exposed to the same quantity of DMSO as
620 drug, for 16 h and harvested for flow cytometry analysis. Flow cytometry analysis was conducted as
621 previously described. Drugs that were tested for further validation after initial screen were: Orantinib
622 (Selleckchem, S1470), Dasatinib (Selleckchem, S7782), Poziotinib (Selleckchem, S7358), Tamoxifen
623 Mylan (Mylan AB*), Erythromycin (Stragen Pharma GmbH*), Naloxone (B. Braun*), Entacapone
624 (Orion Corporation*) and Cinacalcet (Ratiopharm GmbH*). Drugs labeled with "*" were
625 pharmaceutical grade medications gifted from the Pharmacy at Landspítali University Hospital.
626 Analysis was performed as described above.

627 **Apoptosis assay:** We based our apoptosis assay on a protocol published by Xiang et al.[78]. We
628 exposed 293WT+Cas9+SP1 cell line either to 1-5 µM H_2O_2 or vehicle (H_2O) for 4 h at 32˚C or 37˚C. 4 h
629 after exposure gMFI of the cells were analyzed with flow cytometry as described above.

630 **Cell cycle assay**: The cell cycle assay was based on a protocol from Rutgers Flow Cytometry/Cell
631 Sorting & Confocal Microscopy Core Facility (available online)[79]. HEK293 cells were seeded in four 12-
632 well culture plates. The day after, the media was replaced with fresh media containing Poziotinib,
633 Entacapone, or DMSO (vehicle) either at 32 or 37°C. 16 h later, the cells were harvested. To include
634 dead cells in the analysis, the media and the PBS used to wash the cells were collected with the cells.
635 Cells were fixed with 1% paraformaldehyde for 1 hour at 4°C and then permeabilized with 66% EtOH
636 at 4°C for 2 hours. Next, cells were stained with 1 x propidium iodide + RNase staining solution
637 (Abcam, ab139418) and incubated at 37°C in the dark for 30 minutes. Cells were placed on ice and
638 underwent flow cytometry.

639 **Genome Wide CRISPR-Cas9 screen on fluorescent HEK293WT cell lines that stably express SP1-**
640 **MHI:** Using the 293WT+Cas9+SP1 and 293WT+Cas9 (negative control) cell lines we performed a
641 genome wide CRISPR-Cas9 knockout screen (GeCKO) screen, where we transduced the sgRNA pool
642 made from library A and B (Addgene, #1000000049) in MOI 0.3[17–19]. We mostly followed the Joung et
643 al. protocol[19], the exceptions are as follows. For making the lentivirus, a protocol described by Kutner
644 et al.[80] was used. Lentiviral sgRNA library concentration was done with Amicon ultracentrifugal filters
645 (Millipore, UFC9003). 20 h after transduction with the sgRNA library selection was started with
646 Puromycin and continued for 6 days and 8 h before the cells were moved to 32°C, where they were
647 incubated for 16 h before fluorescent activating cell sorting (FACS) with Cell sorter SH800Z (Sony).
648 The 5% highest fluorescent cells for 293WT+Cas9+SP1 and 5% lowest fluorescent cells for
649 293WT+Cas9+SP1 were sorted. Next, we isolated gDNA and performed a two step PCR for all
650 samples (sorted as well as negative control). According to cell number after puromycin selection, the
651 sgRNA library coverage was >700 times coverage for HEK293WT+Cas9+SP1. Next generation
652 sequencing (NGS) was performed with single read, 80 cycles and 8 indexing cycles with PhiX spike in
653 of 20% on NovaSeq 6000 S4 at deCODE genetics for HEK293WT+Cas9+SP1 and HEK293WT+Cas9, 32-
654 280 million aligned reads per sample. To analyze the screen data, single read fastq files for each
655 replicate and condition were merged using cat command. Then, MAGeCK (v.0.5.9) was used to
656 identify enriched sgRNA's in sorted samples[33,81] and sgRNA counts were normalized to internal
657 control for sgRNA's (control sgRNAs). We used RStudio (R, v.4.1.1)[82] to visualize the results and to
658 filter genes. We exported a list of genes that had both FDR value under 0.25 and LFC value over 2.5
659 for each condition in both screens. Then, we excluded genes, overrepresented in both the repressor
660 and activators screen when compared to control as they most likely promote cell growth and
661 therefore were present in both lists (**Supplementary Table 4**). For the pathway enrichment analysis
662 we used EnrichAnalyzer() from MAGeCKFlute (v.1.12.0)[81].

663 **Making of *SMYD5* knockout (*SMYD5*-KO) cells:** Two ready-made sgRNA vectors (Genscript, *SMYD5*
664 plasmid vector #2 and #6) were packed into lentivirus according to protocol described by Kutner et
665 al.[80], for concentration we used the 4x Lentivirus concentrator solution protocol from the MD
666 Anderson Cancer center at University of Texas (available online)[83]. We selected for stable *SMYD5*-KO
667 cells with Puromycin selection for at least 7 days.

668 **Making of *MALT1* and *RGS21* knockout cells**: Ready-made sgRNA vectors (Genscript, plasmid vector
669 *MALT1* #1 and #2, *RGS21* plasmid vector #2 and #3) were packed into lentivirus and selected as
670 described above in the making of *SMYD5-KO* cells.

671 **Making of gRNA resistant SMYD5-Flag plasmid (**Flag-SMYD5 sgRNAres plasmid)**:** In an effort to make
672 SMYD5-Flag resistant to CRISPR-Cas9 cutting from the two guides (Genscript, *SMYD5* plasmid vector
673 #2 and #6), we used site-directed mutagenesis (Q5® Site-Directed Mutagenesis Kit from NEB, E0554S)
674 to modify predicted PAM sites of the guides. We used the following primers to induce the mutations:
675 SMYD5-2mut-F: 5'-gctctttacgAGGAAGCAGTCAGCCAGT-'3; SMYD5-2-mut-R: 5'-
676 ttccgtaaagAGTCTCCGCAGAAGTTCC-'3; SMYD5-6-mut-F: 5'-accgatatcgAGCCTGTGACCACTGCCT-'3;
677 SMYD5-6-mut-R: 5'-atagagcgtt-CCAGAGAAACTGTGCAGCC-'3. After site-directed mutagenesis, we
678 isolated plasmid with Monarch Midiprep kit (NEB, T1010) and Sanger sequenced to verify changes in
679 PAM-sites. This plasmid was then used for rescue experiments (**Figure 4E-4G**).

680 **siRNA:** We used the TriFECTa RNAi kit (IDT; TYE 563 Transfection Control DsiRNA, 51-01-20-19
681 (transfection control); Negative Control DsiRNA, 51-01-14-03 (negative control)) and used
682 predesigned DsiRNA (IDT, hs.Ri.SMYD5.13.8) to knockdown *SMYD5* mRNA in two biological cell lines
683 of HEK293+Cas9+SP1-MHI. For the reverse transfection we used Lipofectamine 2000 (Thermo Fisher
684 Scientific, 11668027) where we seeded $1*10^6$ cells per well in a 6 well plate and exposed to siRNA.
685 Around 24 h after the reverse transfection one batch of cells was exposed to 32°C and the other kept
686 at 37°C for 6 hours before the cells underwent flow cytometry. Further statistical analysis of the flow
687 cytometry data was similar to that described above.

688 **Immunofluorescence of cell culture:** HEK293 cells were seeded into two 8-well chamber slides
689 (Falcon, 354118) and cultured for 24-48 h before one of the chamber slides was moved to 32°C. After
690 6 h cells from both slides at 32°C and 37°C were fixed and permeabilized with 4% PFA and 0.1%
691 Triton-X 100 diluted in PBS for 10 minutes at room temperature. Then cells were washed twice with a
692 blocking solution (PBS with 2.5% BSA and 10% normal goat serum) and followed by blocking for 30
693 min at room temperature in the blocking solution. Cells were incubated overnight with primary
694 antibodies (rabbit anti-SMYD5, 1:1000[51]; anti-FLAG, 1:500, (Sigma-Aldrich, F1804-200UG)) at 4°C. The
695 following day, cells were incubated at room temperature for 30 mins and then washed three times
696 every 10 min with a washing solution composed of PBS with 0.25% BSA. Cells were incubated with
697 secondary antibodies (goat anti-mouse IgG (H+L) Alexa Fluor™ 488, 1:1000 (Invitrogen™, A-11001);
698 goat anti-rabbit IgG (H+L) Alexa Fluor™ 647, 1:1000 (Invitrogen™, A21244)) for 1 h at room
699 temperature in the dark. Cells were washed three times every 10 mins with the washing solution and
700 mounted with Fluoromount-G Mounting Medium with DAPI (Invitrogen, 00-4959-52). Cells were
701 imaged using confocal microscopy (FV 1200, Olympus Fluoroview) using a 30x silicon objective
702 (NA1.05). Images were processed by ImageJ[84,85] and quantified using CellProfiler (v.4.2.5.)[86]. Statistics
703 were calculated in GraphPad Prism.

704 **Real Time Quantitative Polymerase Chain Reaction (RT-qPCR):** Total RNA from cells incubated at 32
705 or 37°C was isolated, using Direct-zol™ RNA Microprep (Zymo Research, R2062) according to the
706 manufacturer's instructions. The concentration of RNA was measured by NanoDrop (Thermo Fisher
707 Scientific) followed by cDNA synthesis with High-Capacity cDNA Reverse Transcription Kit (Applied
708 Biosystems, 4368814) on MiniAmp™ Thermal Cycler (Applied Biosystems™). RT-qPCR was performed
709 using Luna® Universal qPCR Master Mix (NEB, M3003) on CFX384™ Real-Time PCR Detection System

710 (Bio-Rad). Each biological replicate of the RT-qPCR assay in this study was carried out in technical
711 triplicates. Any technical replicate that deviated from other replicates by ≥ 0.4 cycle threshold (Ct)
712 was removed from calculations of average Ct values. The primers used are as follows: SP1 (fwd): 5'-
713 CACCCAATTCAAGGCCTGCCGT-3'; SP1 (rev): 5'-GGGTTGGGCATCTGGGCTGTTT-3'; RBM3 (fwd): 5'-
714 GAGACTCAGCGGTCCAGGGGTT-3'; RBM3 (rev): 5'-CCTCTGGTTCCCCGAGCAGACT-3'; CIRBP (fwd): 5'-
715 CCGAGTTGACCAGGCTGGCAAG-3'; CIRBP (rev): 5'-TCCATAGCCCCGGTCTCCTCCT-3'; GAPDH (fwd): 5'-
716 TCAAGGCTGAGAACGGGAAG-3'; GAPDH (rev): 5'-CGCCCCACTTGATTTTGGAG-3'. SMYD5 1 (fwd): 5'-
717 GCACTGTGCGCAAAGACCTCCA-3', SMYD5 2 (fwd): 5'-GGAAACCAGGCCAGGTTCTGCC-3', SMYD5 3
718 (fwd) 5'-CGTGGAAGTCCGTTTCGTGA-3', SMYD5 1 (rev:) 5'-CTGGGCACAGGACCTGGTGGTA-3', SMYD5
719 2 (rev): 5'-GGCTGCCAACCGACATTCTGCA-3', SMYD5 3 (rev) 5'-CCAGAGAAACTGTGCAGCCA-3'.

720 **Western blot assay:** Cells were washed with PBS and then lysed (whole cell lysate) for 30 min on ice
721 in RIPA buffer (50mM Tris HCl ph8, 150mM NaCl, 1% NP-40, 1% Sodium deoxycholate, 0.1% SDS,
722 2mM EDTA, phosphatase inhibitor (either Cell signaling, 5870S or Thermo Fisher Scientific, 78437)).
723 The lysate was centrifuged at 16,000 xg for 20 min at 4°C and the supernatant was collected. The
724 supernatant was diluted with 4X loading buffer (LI-COR, 928-40004) and heated at 95°C for 5 min.
725 The protein concentration was measured using Pierce™ BCA Assay Kit (Thermo Fisher Scientific,
726 23225). 20-30 µg of protein was loaded into each well and separated by SDS-PAGE. They were
727 transferred to polyvinylidene fluoride (PVDF) membranes and blocked in 5% bovine serum albumin in
728 Tris-buffered saline with Tween 20 for 1 h. Primary antibodies: rabbit anti-CIRBP, 1:2000
729 (Proteintech, 10209-2-AP); rabbit anti-RBM3, 1:1000 (Proteintech, 14363-1-AP); rabbit anti-SP1
730 1:1000 (Proteintech, 21962-1-AP); mouse anti-Lamin B1, 1:5000 (Proteintech 66095-1-Ig); rabbit anti-
731 SMYD5, 1:1000[51]; mouse anti-GAPDH, 1:5000 (Abcam, ab8245) were applied to respective
732 membranes after washing, and incubated at 4˚C overnight. Membranes were incubated with IRDye®
733 secondary antibodies; anti-rabbit (LI-COR,926-32213); anti-mouse (LI-COR, 926-68072), at room
734 temperature for 90 mins. After washing, the protein bands were visualized on the Odyssey® CLx
735 Infrared Imaging System and protein band intensity quantified by Image J[84,85] software.

736 **DNAm studies and analysis:** HEK293WT (biological triplicates) were split into two batches and
737 exposed to 37°C and 32°C for 6 h, next cells were harvested, and DNA isolated with the Zymo Quick-
738 DNA™ Midiprep Plus Kit (Zymo Research, D4075). Samples were submitted to the Genetic Resources
739 Core Facility (Johns Hopkins University), bisulfite treated, and run on the Infinium MethylationEPIC
740 BeadChip Kit (Illumina) with two technical controls (50% and 100% DNAm, 8 samples total). Technical
741 controls were created using mixtures of 100% and 0% methylated HCT116 DKO (Zymo Research
742 D50414-1/2). DNA methylation data (IDAT files) containing unmethylated and methylated intensity
743 values were imported to R (v.4.2.1) for analysis[82]. Raw data was processed using single sample
744 approach with preprocessNoob() function and methylation values (beta values) were obtained using
745 the getBeta() function from minfi package (v.1.42.0)[87–89]. The model matrix was created for the two
746 temperatures using the model.matrix() function from stats R package and sva() function from sva
747 package (v.3.44.0) was applied with two estimated surrogate variables[82,90]. The model was fit with
748 contrast matrix using lmFit(), with the estimated coefficients and standard errors generated using
749 contrasts.fit() from limma package (v.3.52.4)[91]. The p-values were moderated using eBayes() function
750 from limma package (v.3.52.4) and CpG cites ranked according to their p-value[91].

751 **CUT&RUN:** 293WT and human NPCs (ATCC, ACS-1019) were harvested after 6 h at 32°C or kept at
752 37°C. CUT&RUN performed according to Epicypher CUTANA protocol (v.1.7)[92] on 300.000 cells per

753 sample. We permeabilized the cells with 0.01% digitonin (Sigma, D141). For normalization we spiked
754 in E. Coli DNA (Epicypher, 23618-1401) at the final concentration of 0.2 ng per sample. The library
755 preparation was performed with TrueSeq-Chip Sample preparation Kit (Illumina, IP-202-9001). The
756 following antibodies were used for the CUT&RUN: CTCF antibody (Cell Signaling, 2899S), H3K36me3
757 (Thermo Fisher Scientific, MA5-24687), H4K20me3 (EpiCypher, 13-0054), H3K9me3 (Abcam,
758 ab176916), H3K4me3 (EpiCypher, 13-0041), H3K27me3 (Thermo Fisher Scientific, MA5-11198),
759 SMYD5 [51], and Rabbit IgG Antibody (Epicypher, 23613-0042). The sequencing was performed on a
760 NovaSeq 6000 S4 at deCODE genetics, paired-end 8 cycles of index1, 8 cycles of index 2, 150 cycles
761 read 1 and, 150 cycles read 2, where we aimed for 10 million reads per sample. For the CUT&RUN
762 analysis and the CUT&TAG re-analysis we followed published STAR protocols[93]. Briefly, first we
763 trimmed the raw Fastq reads in paired mode with TrimGalore (v.0.6.7)[94] then we used Bowtie2
764 (v.2.4.4.)[95] to align the reads to Hg38 or mm10 and E. Coli reference genome, all downloaded from
765 UCSC. Overall alignment to Hg38 were from 83.6-98.63% and to E. Coli spike in were from 0.1-4.18%
766 for our data. The aligned Sam files were then converted to Bam files, indexed, and sorted via
767 SAMtools (v.1.15)[96] and BedGraphtoBigWig (v.4)[97] from BEDTools (v.2.3)[98]. We used SEACR (v.1.3)[99]
768 for peak calling after normalization with the normalization factor calculated as 1/(percent alignment
769 to E. coli). We used DiffBind (v.3.9.6)[100] for the differential peak analysis, ChIPseeker (v.1.35.3)[101],
770 TxDb.Hsapiens.UCSC.hg38.knownGene (v.3.4.6)[102] and org.Hs.eg.db (v.3.8.2)[103] for annotation. For
771 further analysis and image creation we used deepTools (v.3.5.1.)[104] and R [82].

772 **Mouse NPC isolation:** Mouse NPCs were isolated from the cortex of E17.5 C57BL6/NTac embryos.
773 The protocol was adapted from Bernas et al, 2017[105]. Embryo cortices were manually dissected from
774 brains and the tissue was dissociated in 1X TrypLE™ Select Enzyme (Thermo Fisher Scientific,
775 A1217701) for 10 min, with manual dissociation using a 1000 µL pipette. The cell suspension was
776 washed in Neurobasal medium (Thermo Fisher Scientific, 21103049) and filtered through a 70 µm
777 cell strainer (Miltenyi Biotech, 130-110-916). Cells were washed twice in 5 mL Neurobasal medium
778 (Gibco, 21103049) by centrifugation at 200 xg for 10 min. Cells were resuspended in 1 mL Neurobasal
779 growth medium containing 1X B27 supplement (Thermo Fisher Scientific, 17504044), 1X
780 Penicillin/Streptomycin (Thermo Fisher Scientific, 15140122), 1X Glutamax (Thermo Fisher Scientific,
781 35050038), 20ng/mL FGF-2 (Peprotech, 100-18B), 20 ng/mL EFG (Peprotech, AF-100-15), and 2
782 µg/mL Heparin (MP Biomedicals, 210193125). Cells were seeded onto 12-well plates, previously
783 coated for 2 h at 37°C in 1:100 dilution of Matrigel (Corning, 354234). After passaging, NPCs were
784 cultured in media described above on plates coated overnight in poly-D-lysine (Sigma, P7280), and
785 then coated for 2 h in laminin (Sigma, L2020). Cells were either sub-cultured or media was changed
786 every 2 days.

787 **RNAseq:** Primary mouse NPC lines from 4 separate embryos were seeded 0.3 x 10^6 cells per well, in
788 two batches, in a poly-D-lysine/laminin coated 6-well plate after 9 days *in vitro*. Following 36 h of
789 incubation at 37°C, one plate with 4 lines was incubated at 32°C for 6 h. Cells from both 37°C and
790 32°C conditions were harvested in tri-reagent and RNA was isolated using the Direct-zol RNA
791 Microprep kit (Zymo Research, R2063). RNAseq library construction and Illumina next generation
792 paired-end sequencing was performed by Novogene, generating 30 million paired-end reads per
793 sample. For the RNAseq analysis, Fastq files were pseudo-aligned to the GRCm39 mouse
794 transcriptome, downloaded from NCBI, using Kallisto (v.0.48.0) with paired-end mode on and 100
795 bootstraps. Kallisto output files were imported into R using the tximport package[106]. Transcripts were
796 assigned to genes using the TxDb.Mmusculus.UCSC.mm10.ensGene package (v.3.4.0) [107] in R .

797 Differential expression analysis was performed using the DESeq2 package (v.3.16)[108] in R, after
798 discarding transcripts with less than 10 counts. Differentially expressed genes were defined as those
799 with an adjusted p-value less than 0.1. Overlaps of gene lists were calculated using the GeneOverlap
800 package (v.1.34.0)[109] in R, with overlaps tested using Fisher's exact test. Gene set enrichment analysis
801 was performed using the GSEA-preranked program[110,111] with the Mouse Ortholog Hallmark Gene
802 Sets[112]. For the GSEA-pre-ranked run, we generated a ranked gene list comprising all detected genes
803 assigned to a rank value, which was calculated as -log10(adjusted p-value) × (sign of fold change).
804 The genes were then ranked from the highest rank value to the lowest before inputting into the
805 program.

806 **Mouse cooling followed by immunostaining on brain slices:** C57BL6 mice (Jackson) were bred to
807 create a litter (n=2). At P10, we split littermates into two groups. One group (n=6) was cooled to a
808 core temperature of 32°C and the other (n=6) maintained at 37°C, for 6 hours respectively. These
809 animals were then euthanized, and their brains were isolated immediately after the cooling period
810 and flashed with PBS. One of the hemispheres was immersed in 4% PFA for 72-96 h for fixation and
811 the other hemisphere was dissected for the cerebellum, thalamus/basal ganglia, hippocampus,
812 anterior and posterior cortex. After fixation, samples were cryopreserved in a sucrose gradient and
813 then flash-frozen. Frozen hemispheres were cryosectioned with the help of a cryostat (Keldur, UI).
814 The sections were washed in TBS+ (TBS (LiCor, 927-60001) with 0.05% triton X-100 (Sigma-Aldrich,
815 T8787-100ML)) twice for 10 minutes. Next, the slides were immersed in DAKO (target retrieval
816 solution, sodium citrate buffer, pH 6) at 95°C for 20 minutes. Slides were then washed again in TBS+
817 twice for 10 minutes. Next, the slides were blocked in TBS++ (TBS (LiCor, 927-60001) with 3% goat
818 serum (Abcam, ab7481)) for 1 h at room temperature. The slides were then stained with primary
819 antibodies and anti-rabbit-SMYD5[51], 1:200, for 24 h at room temperature and carried out in the dark.
820 On the next day, slides were allowed to reach room temperature before they are washed 3x for 10
821 minutes in TBS+. The slides were incubated with secondary antibodies, goat anti-mouse IgG (H+L)
822 Alexa Fluor™ 488, 1:1000 (Invitrogen™, A-11001); goat anti-rabbit IgG (H+L) Alexa Fluor™ 647, 1:1000
823 (Invitrogen™, A21244), for 24 h in the dark and washed 3x for 10 minutes in TBS+. All the liquid on
824 the slides was briefly dried off. Fluoromount-G Mounting Medium with DAPI (Invitrogen, 00-4959-52)
825 was placed on each section and covered with a cover slip. The slides were incubated for 24 h at room
826 temperature before being imaged using confocal microscopy (FV 1200, Olympus Fluoroview) using a
827 30x silicon objective (NA1.05). Images were processed by ImageJ[84,85] and quantified using CellProfiler
828 (v.4.2.5.)[86]. Statistics were calculated in GraphPad Prism.

829

830 **Supplementary Tables, Files and Figure titles and legends**

831 **List of Supplementary Tables.** All Word documents.

832 **Supplementary Table 1**: Specifics of our MHI, including sequence material used, vector, selection
833 markers, plasmid size and individual fluorophores.

834 **Supplementary Table 2**: Top 91 drug hits from MHI screen.

835 **Supplementary Table 3**: Top candidate genes found enriched in mutation screening.

836 **Supplementary Table 4:** Genes found in both repressor and activator SP1 lists and thus excluded for
837 further evaluation.

838 **Supplementary Table 5**: List of CpGs represented at three genes.

839 **Supplementary Table 6**: List of differentially methylated locations from EPIC DNAm array.

840 **Supplementary Table 7:** Top differentially modified locations for H3K36me3 in NPCs from CUT&RUN
841 experiment.

842 **Supplementary Table 8:** List of genes that have a unique H3K4me3 histone modification peak at
843 32°C.

844 **Supplementary Table 9**: List of genes that show DEGS at 32°C and have a unique H3K4me3 histone
845 modification peak at 32°C.

846 **List of Supplementary Files.** Word document.

847 **Supplementary File 1:** Sequences of individual MHIs.

848

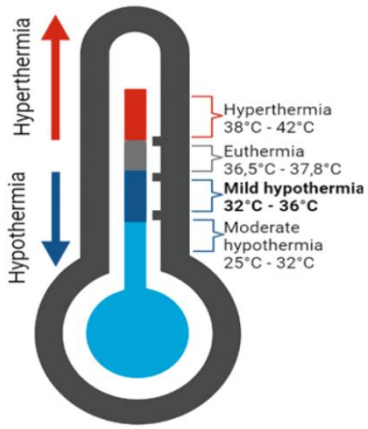

Figure S1. Different temperature ranges. Temperatures known to induce distinct responses (moderate and mild hypothermia, euthermia and hyperthermia). Our range of interest (mild hypothermia) is bolded.

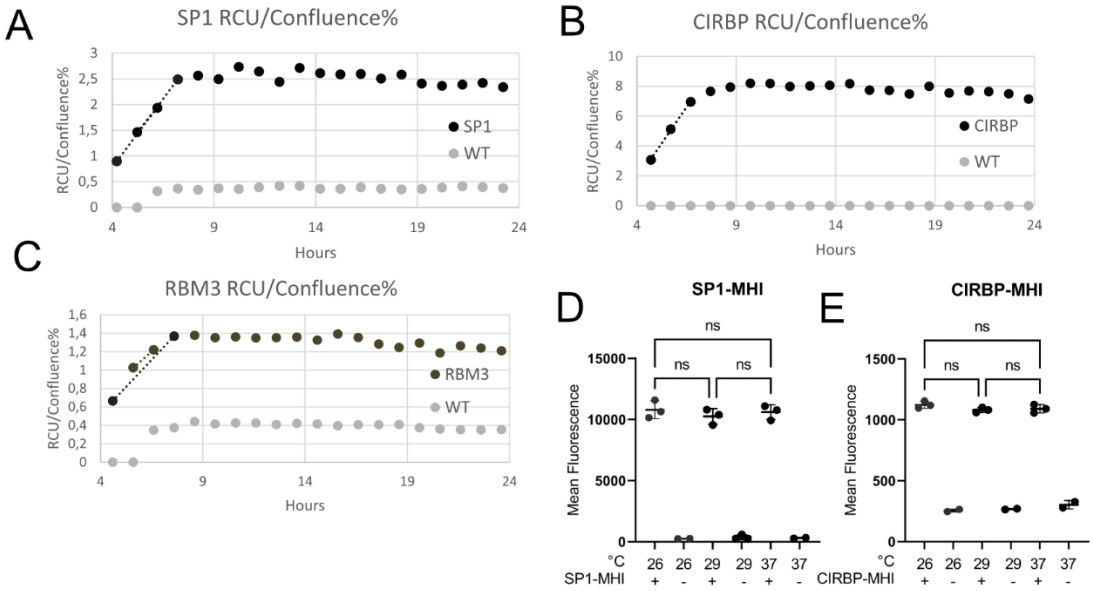

854

855 **Figure S2. MHI activation peaks during mild hypothermia (32˚C) and is limited at other**
856 **temperatures.** (A-C) We measured fluorescence hourly using an IncucyteS3 at 32°C using SP1-Lenti-
857 MHI, CIRBP-Lenti-MHI, RBM3-Lenti-MHI respectively. (D-E) No increased fluorescence was observed
858 at moderate hypothermia for either SP1-MHI or CIRBP-MHI in HEK293 cells. * = P<0.05, ** = P<0.01,
859 *** = P<0.001, **** = P<0.0001.

860

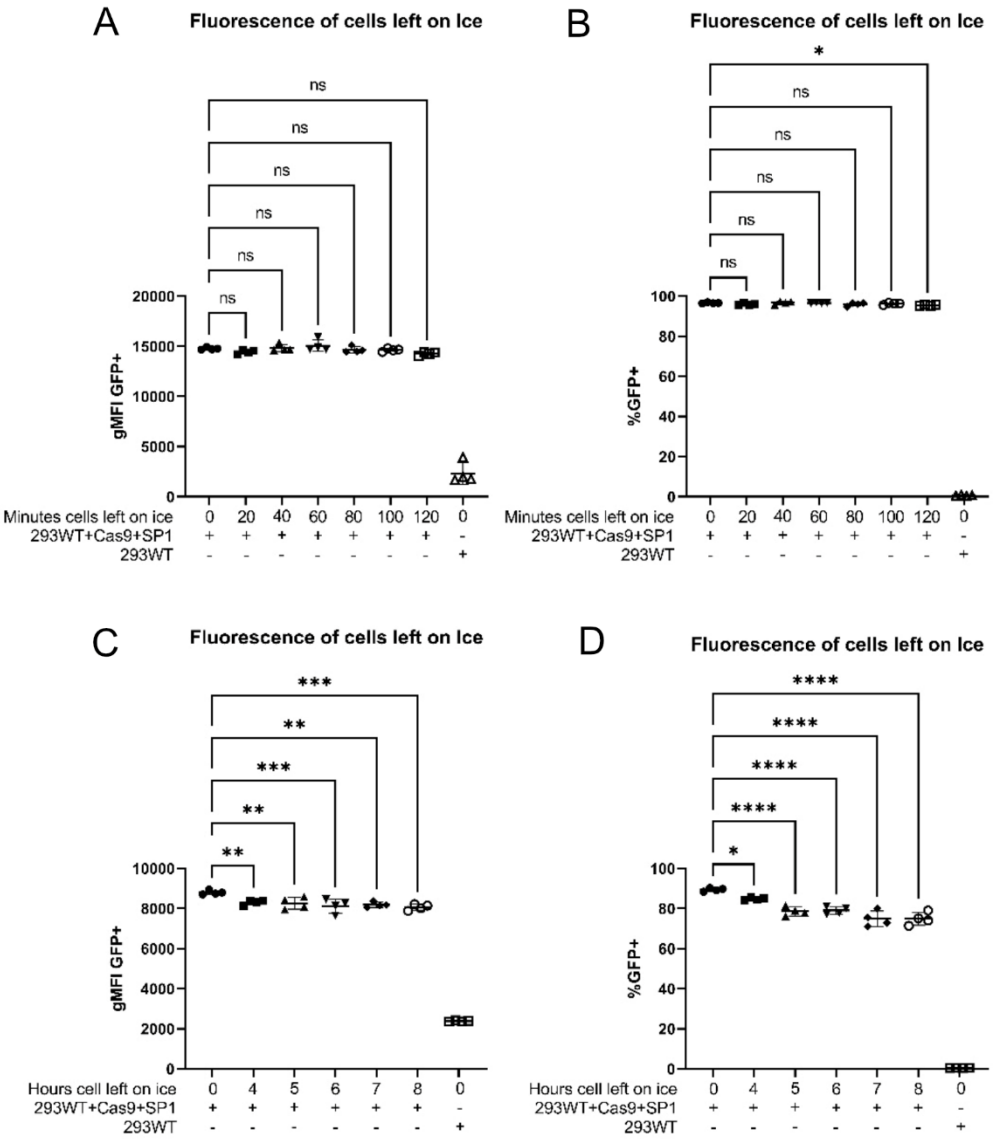

Figure S3. Storage of samples on ice does not lead to activation of MHI. (A-D) gMFI or percentage of fluorescent cells of HEK293WT+Cas9+SP1 left on ice for different periods of time before flow cytometry analysis. Shown are data points, each data point is a technical replicate, mean and SD where applicable. Dunnett's multiple comparison test calculated in GraphPad Prism. * = P<0.05, ** = P<0.01, *** = P<0.001, **** = P<0.0001.

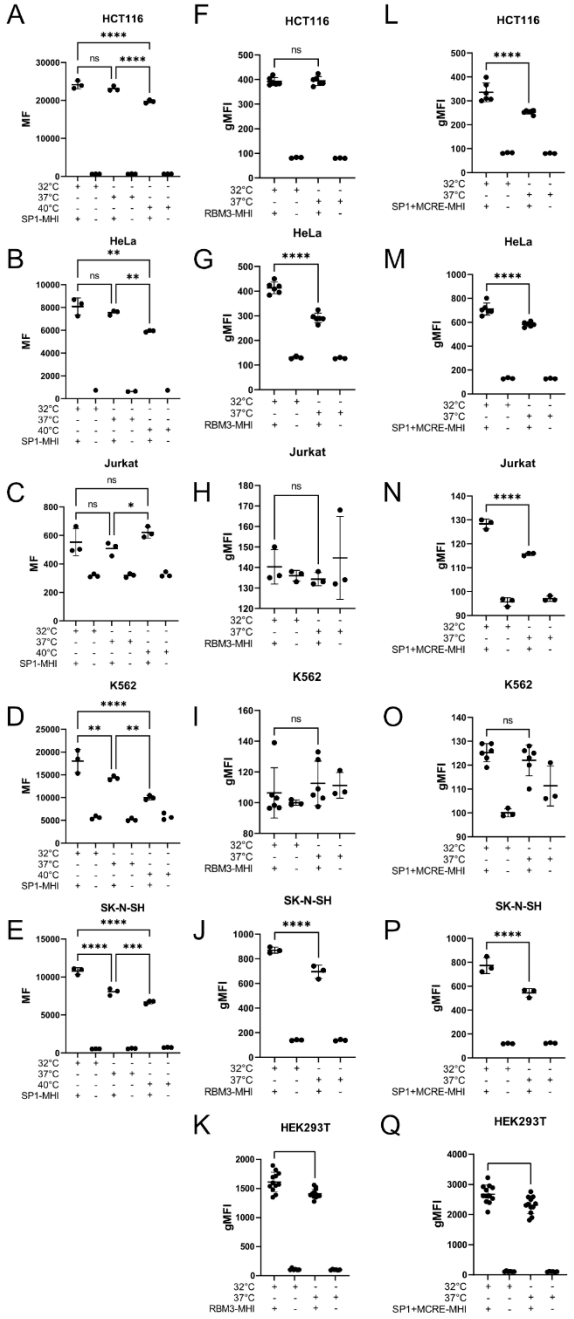

868

869 **Figure S4. MHI demonstrate consistent activation at 32°C in diverse cellular systems.** (A-E) Left
870 column shows mean fluorescence (MF, flow cytometry) after transient transfection of SP1-MHI into
871 HCT116, HeLa, Jurkat, K562 and SK-N-SH (16 h at 32°C, 37°C and 40°C). Shown are data points, each
872 data point is a technical replicate, mean and SD where applicable, Šidák's multiple comparison test
873 calculated in GraphPad Prism. (F-K) Middle column shows gMFI (flow cytometry) after transient
874 transfection of RBM3-MHI into HCT116, HeLa, Jurkat, K562, SK-N-SH, and HEK293T, 16 h at 32°C.
875 Shown are data points, each data point is a technical replicate, mean and SD where applicable,
876 Tukey's multiple comparison test calculated in GraphPad Prism. (L-Q) Right column shows gMFI (flow
877 cytometry) after transient transfection of SP1+MCRE-MHI into HCT116, HeLa, Jurkat, K562, SK-N-SH,
878 and HEK293T, 16 h at 32°C. Data as in (F-K). * = P<0.05, ** = P<0.01, *** = P<0.001, **** = P<0.0001.

879

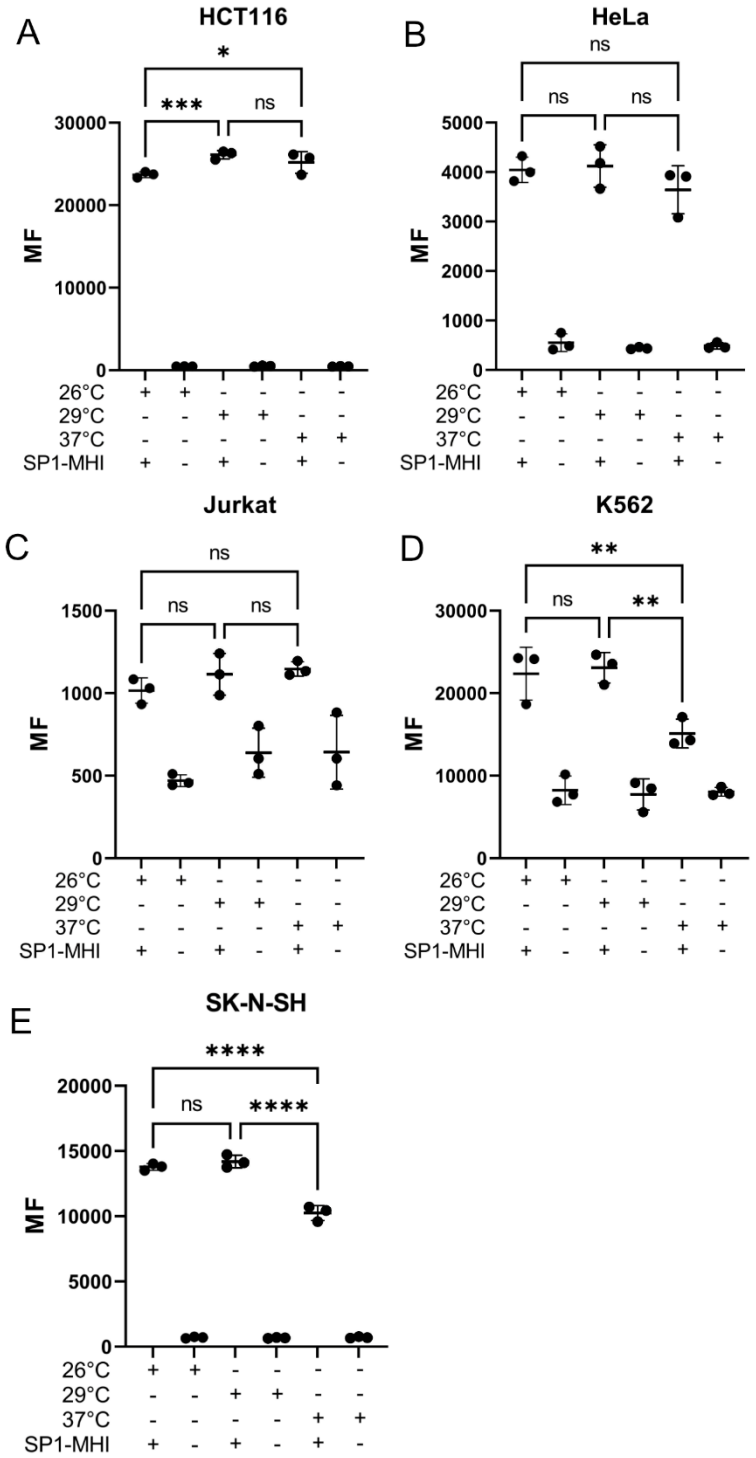

Figure S5. Moderate hyperthermia does not activate SP1 MHI in diverse systems. (A-E) Mean fluorescence of SP1-MHI as measured by flow cytometry after transient transfection of MHI into HCT116, HeLa, Jurkat, K562, and SK-N-SH, 16 h at 26°C or 29°C. Shown are data points, each data point is a technical replicate, mean and SD where applicable. Significance levels calculated with Šidák's multiple comparison test in GraphPad Prism. * = P<0.05, ** = P<0.01, *** = P<0.001, **** = P<0.0001.

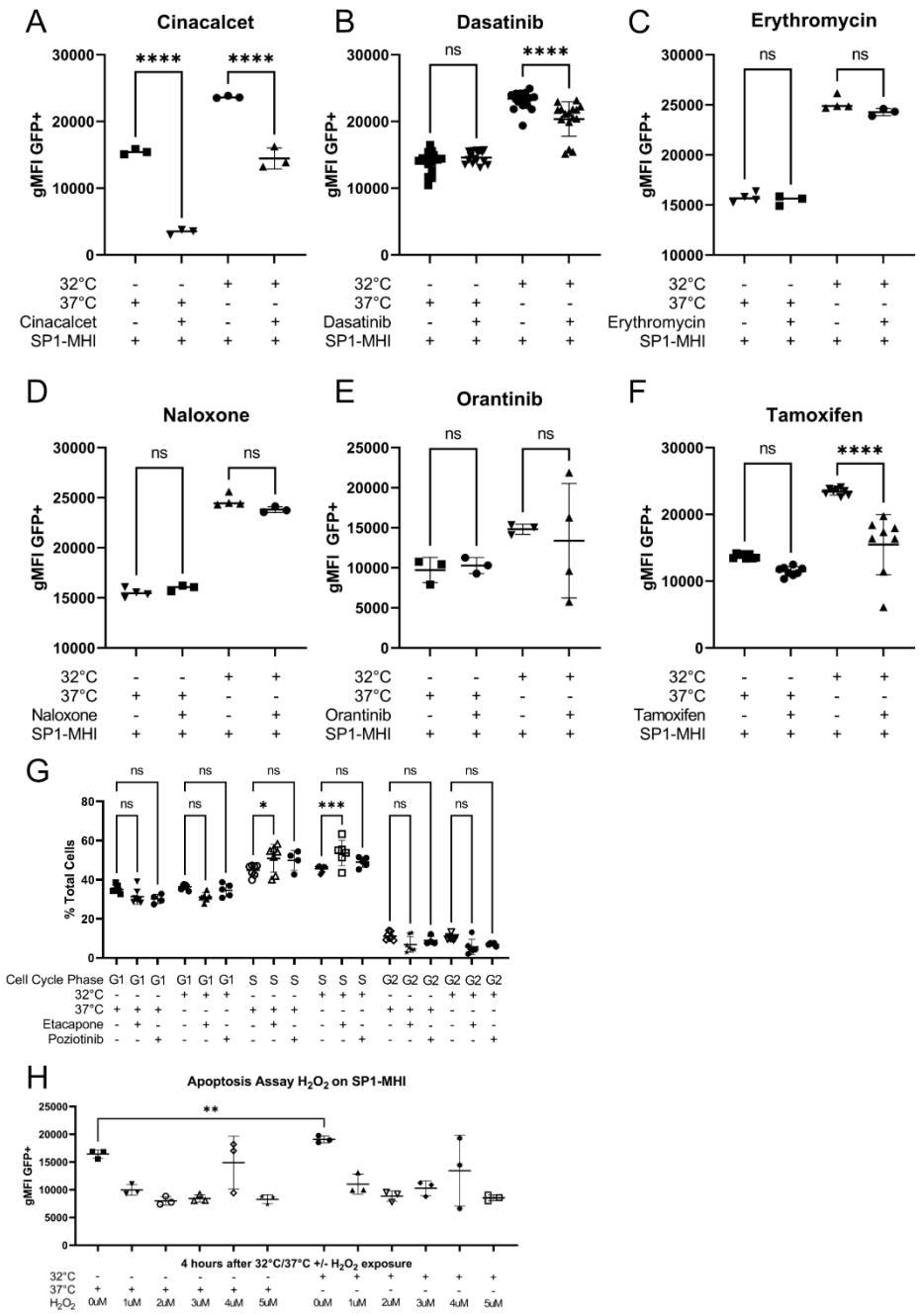

Figure S6: Validation of potential compound hits from drug screen and cell cycle analysis. (A-F) gMFI measured with flow cytometry of HEK293WT cell line that stably expresses SP1-MHI after 16 h of Cinacalcet (A), Dasatinib (B), Erythromycin (C), Naloxone (D), Orantinib (E), and Tamoxifen (F) at 32°C or 37°C. Shown are data points, mean and SD where applicable. Significance levels calculated with Šidák's multiple comparison calculated with GraphPad Prism. (G) Cell cycle analysis done with PI staining. Mean fluorescence measured for G1, S and G2 phases of the cell cycle with flow cytometry of HEK293WT cell line 16 h after Entacapone or Poziotinib exposure at 32°C or 37°C. Data shown as in (A-F). (H) Apoptosis induction analysis done with H_2O_2 exposure. Shown are data points, each point a technical replicate, mean and SD where applicable. Significance levels calculated with an unpaired two-tailed t-test calculated in GraphPad Prism. * = P<0.05, ** = P<0.01, *** = P<0.001, **** = P<0.0001.

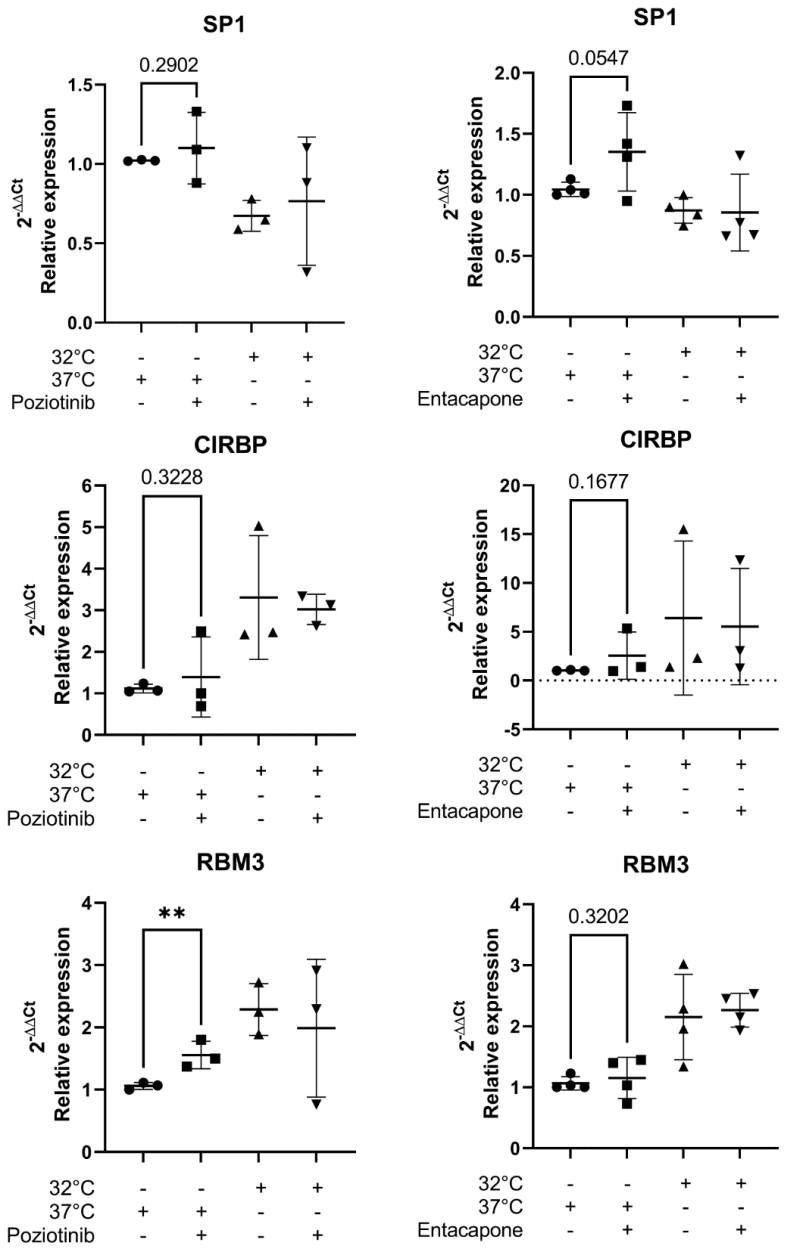

Figure S7: Expression of endogenous loci after exposure to Entacapone and Poziotinib. Relative expression of *SP1* (top), *CIRBP* (middle), *RBM3* (bottom) when compared to GAPDH after 16 h at 32°C or 37°C with and without Entacapone (right) or Poziotinib (left). Shown are data points, each data point is a biological replicate (mean of technical replicates), mean and SD where applicable. Significance levels were calculated with an unpaired one-tailed t-test in GraphPad Prism. * = P<0.05, ** = P<0.01, *** = P<0.001, **** = P<0.0001.

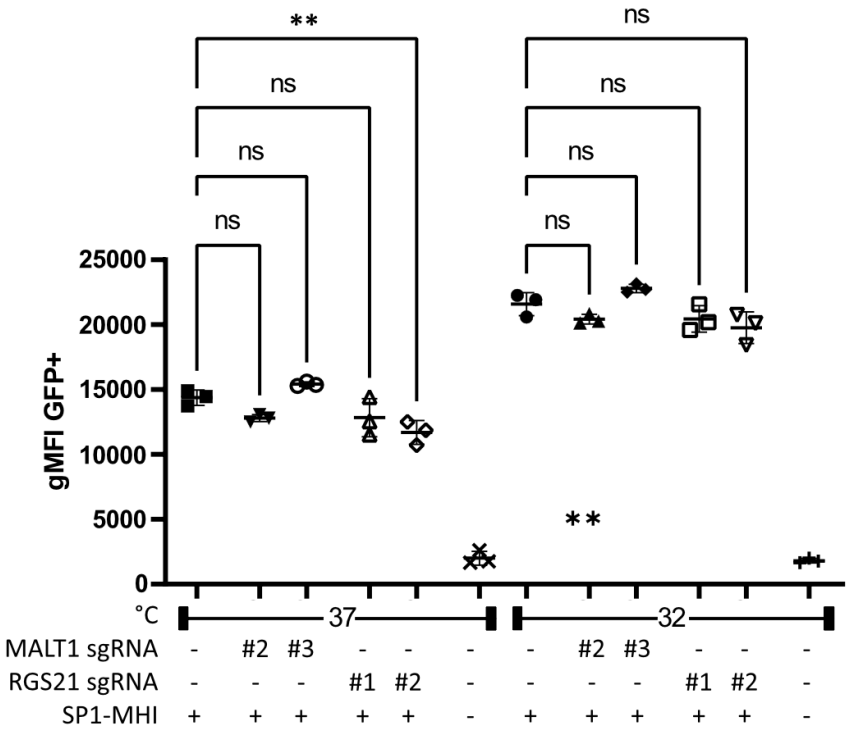

908

909 **Figure S8: *RGS21* and *MALT1* knockout did not show any significant fluorescent change.** sgRNA KO
910 for *MALT1* and *RGS21* did not show any changes in fluorescence of HEK293 cells with SP1-MHI,
911 suggesting that *MALT1* and *RGS21* do not have an impact on SP1-MHI. Shown are data points, each
912 data point is a technical replicate, mean and SD where applicable. Significance levels were calculated
913 with Šidák's multiple comparison test in GraphPad Prism. * = P<0.05, ** = P<0.01, *** = P<0.001,
914 **** = P<0.0001.

915

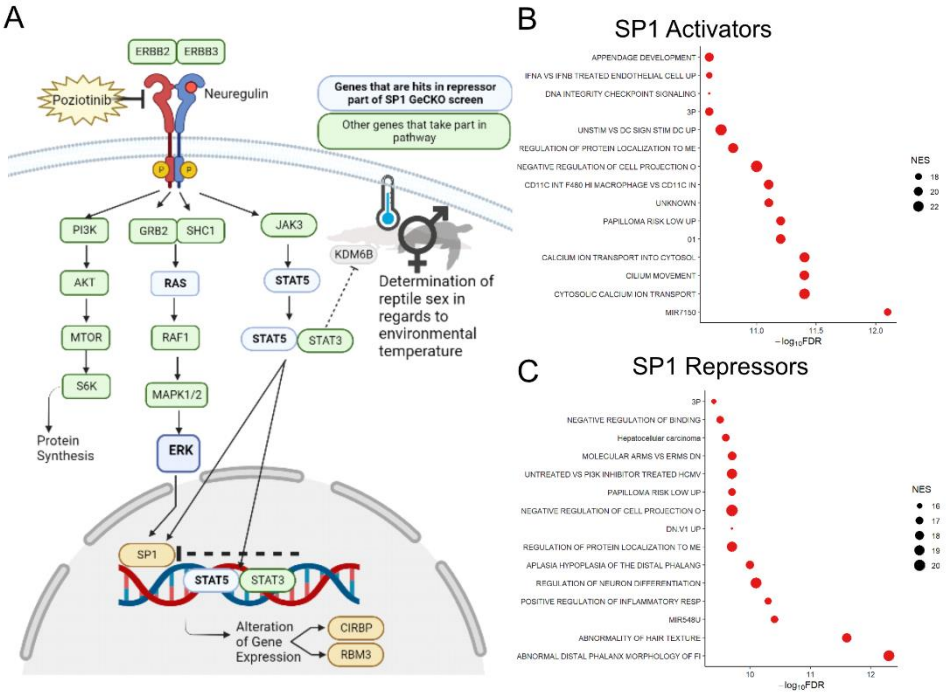

Figure S9. Pathway analysis using genes from forward mutagenesis. (A) Schematic depiction of repressors identified which land on the Neuregulin pathway. (B-C) Unbiased MSigDB pathway enrichment of highly ranked (-Log10(RRA) >0.5) genes from the SP1 activator (B) and SP1 repressor (C) lists.

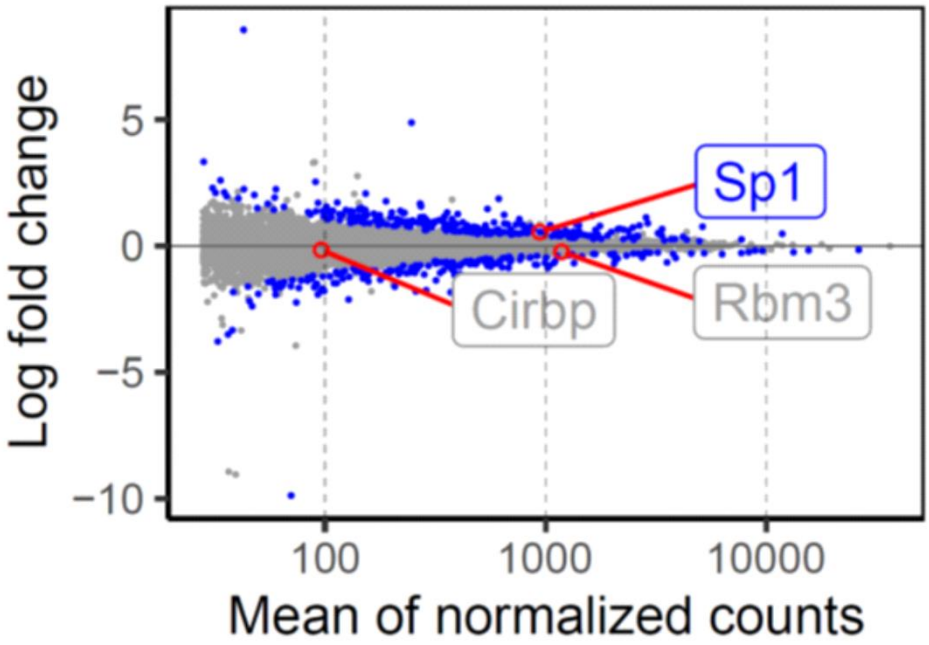

922

923 **Figure S10. *Cirbp* has fewer normalized counts compared to *Sp1* and *Rbm3.*** Normalized counts from
924 RNAseq in mESc (referring to data from **Figure 4C**).

925

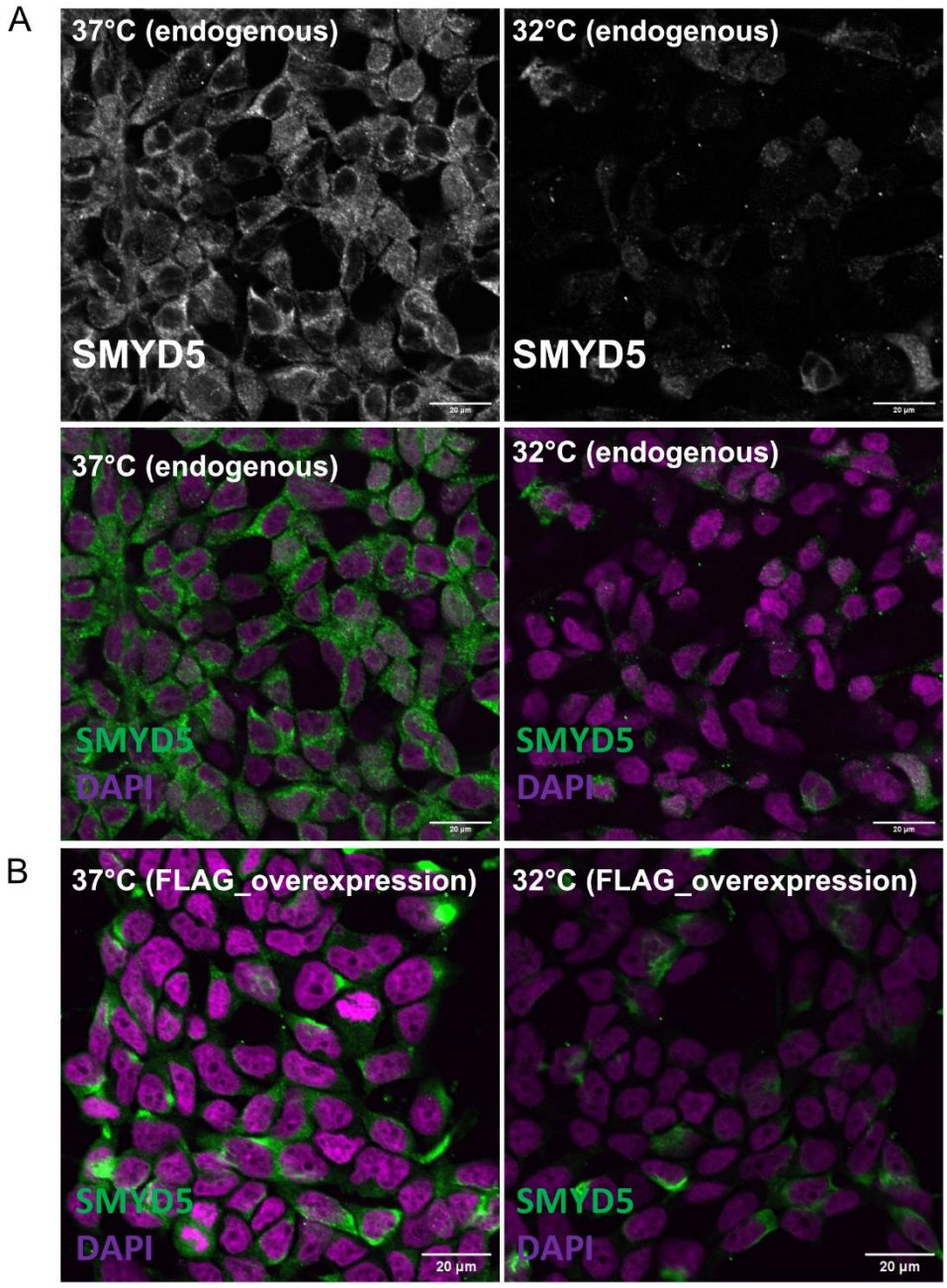

Figure S11. Validation of temperature dependence of SMYD5. (A) An independent biological replicate with anti-SMYD5 antibody showing striking differences between two temperatures. Green or white (SMYD5), purple (DAPI). (B) A validation with anti-FLAG antibody, showing the same difference at the two temperatures. Green (SMYD5), purple (DAPI).

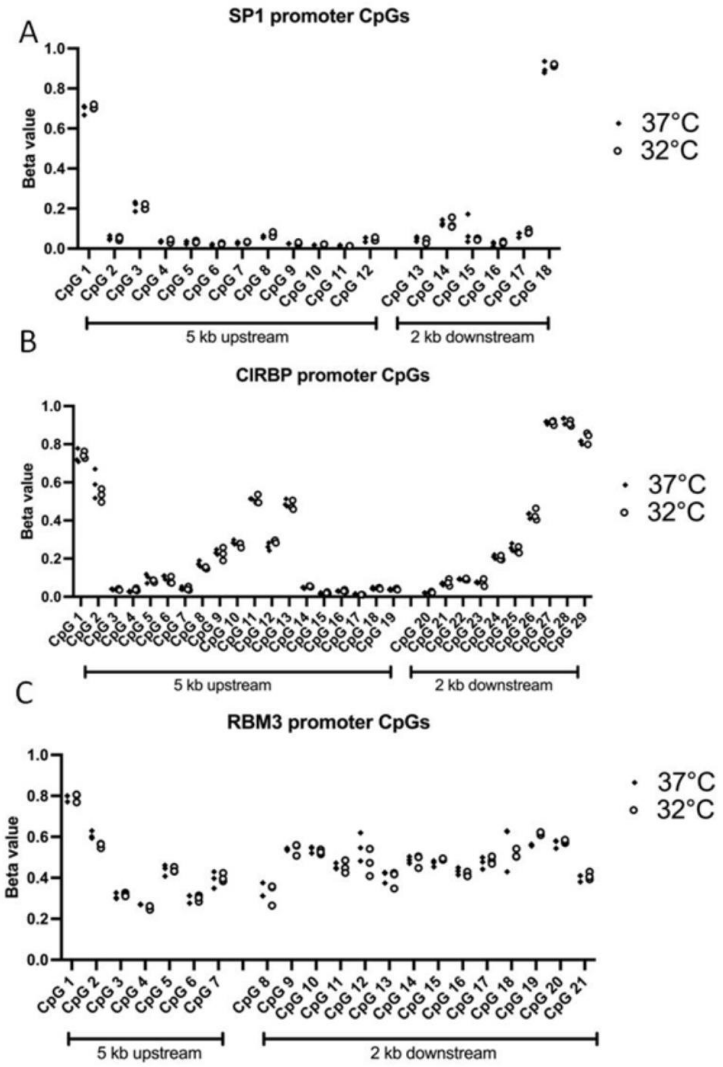

932

933 **Figure S12. DNAm status at *SP1*, *CIRBP* and *RBM3* promoters.** (A) DNAm status of CpG dinucleotides
934 from Illumina EPIC array 5 kb upstream and 2 kb downstream of *SP1* gene. (B) DNAm status of CpG
935 dinucleotides from Illumina EPIC array 5 kb upstream and 2 kb downstream of *CIRBP* gene. (C) DNAm
936 status of CpG dinucleotides from Illumina EPIC array 5 kb upstream and 2 kb downstream of *RBM3*
937 gene.

938

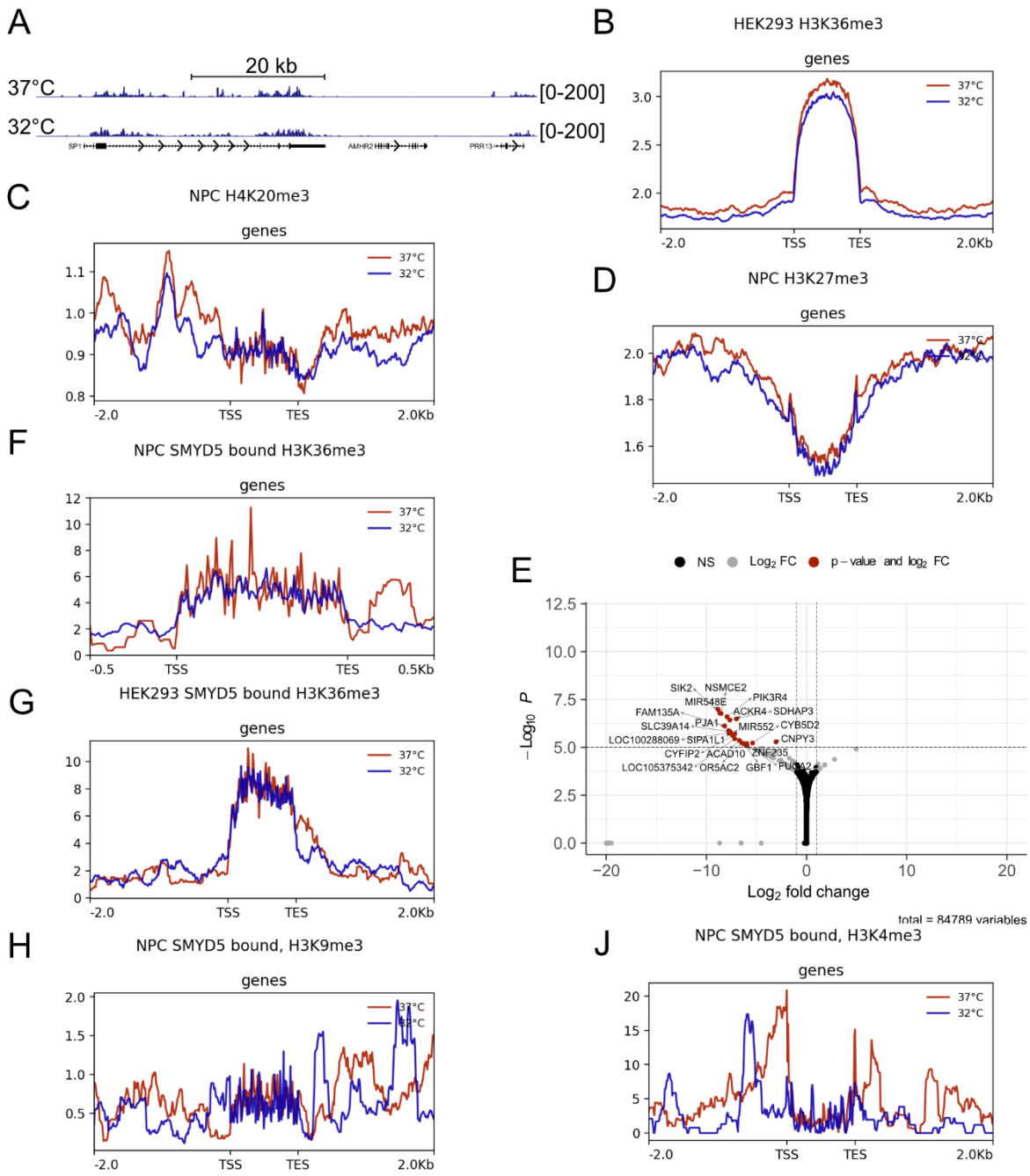

Figure S13. Methylation modification levels in NPCs and HEK293 cells. (A) H3K36me3 levels at 32°C and 37°C at *SP1* promoter in HEK293 cells. (B) Global H3K36me3 levels (all genes) in HEK293 cells. (C-D) Global H3K27me3, H4K20me3 levels, respectively (all genes) in NPCs (E) At the gene-specific levels there is a number of genes, which have more or less H3K36me3 at 32°C compared to 37°C in HEK293 cells. Red circles indicate genes that have Log2 fold change over 1 and p-value less than 10-6, gray circles indicate Log2 fold change over 1 but non-significant p-value (>10-6) and black circles indicate non-significant Log2 fold change and p-values for those genes. (F-G) H3K36me3 levels at SMYD5-bound genes identified to be DEGS at the two temperatures in NPC and HEK293 cells, respectively. (H-J) H3K9me3 and H3K4me3, respectively, levels at SMYD5-bound genes identified to be DEGS at the two temperatures in NPCs.

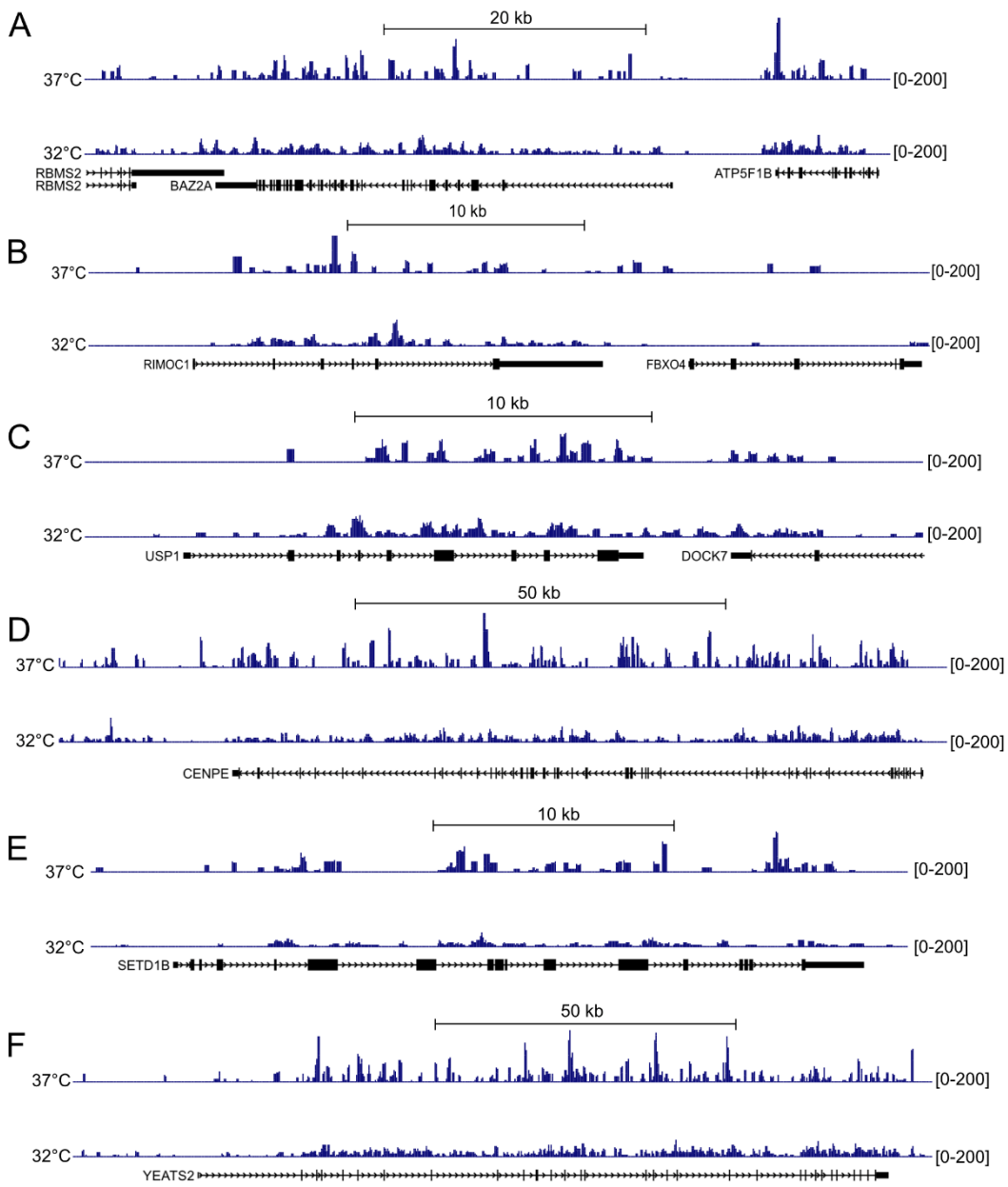

Figure S14: H3K36me3 levels on representative peaks showing differential binding at 32°C when compared to 37°C. (A-C) Increased H3K36me3 is observed for *BAZ2A*, *RIMOC1 and USP1,* respectively, at 32°C compared to 37°C in NPCs. (D-E) Decreased H3K36me3 is observed for *CENPE*, *SETD1B* and *YEATS2I,* respectively, at 32°C compared to 37°C in NPCs.

955 **References**

956 1. Osilla, E. V., Marsidi, J.L., and Sharma, S. (2022). Physiology, Temperature Regulation
957 (StatPearls Publishing).

958 2. Turbill, C., Bieber, C., and Ruf, T. (2011). Hibernation is associated with increased survival and
959 the evolution of slow life histories among mammals. Proceedings of the Royal Society B:
960 Biological Sciences *278*, 3355–3363. 10.1098/RSPB.2011.0190.

961 3. Mathew, J.L., Kaur, N., and Dsouza, J.M. (2022). Therapeutic hypothermia in neonatal hypoxic
962 encephalopathy: A systematic review and meta-analysis. J Glob Health *12*.
963 10.7189/JOGH.12.04030.

964 4. Luedke, M.W., Graffagnino, C., McKinney, B.G., Piper, J., Iversen, E., and Kolls, B. (2022).
965 Association of time-temperature curves with outcomes in temperature management for
966 cardiac arrest. BMJ Neurol Open *4*. 10.1136/BMJNO-2022-000273.

967 5. Dietrichs, E.S., and Dietrichs, E. (2015). Neuroprotective effects of hypothermia. Tidsskr Nor
968 Laegeforen *135*, 1646–1651. 10.4045/tidsskr.14.1250.

969 6. Sun, Y.J., Zhang, Z.Y., Fan, B., and Li, G.Y. (2019). Neuroprotection by Therapeutic
970 Hypothermia. Front Neurosci *13*. 10.3389/FNINS.2019.00586.

971 7. Fujita, J. (1999). Cold shock response in mammalian cells. J Mol Microbiol Biotechnol *1*, 243–
972 255.

973 8. Zhu, X., Bührer, C., and Wellmann, S. (2016). Cold-inducible proteins CIRP and RBM3, a unique
974 couple with activities far beyond the cold. Cellular and Molecular Life Sciences, 1–21.
975 10.1007/s00018-016-2253-7.

976 9. Ryu, H., Lee, J., Olofsson, B.A., Mwidau, A., Deodoglu, A., Escudero, M., Flemington, E.,
977 Azizkhan-Clifford, J., Ferrante, R.J., and Ratan, R.R. (2003). Histone deacetylase inhibitors
978 prevent oxidative neuronal death independent of expanded polyglutamine repeats via an Sp1-
979 dependent pathway. Proc Natl Acad Sci U S A *100*, 4281–4286. 10.1073/PNAS.0737363100.

980 10. Yang, H.J., Zhuang, R.J., Li, Y.B., Li, T., Yuan, X., Lei, B.B., Xie, Y.F., and Wang, M. (2019). Cold-
981 inducible protein RBM3 mediates hypothermic neuroprotection against neurotoxin rotenone
982 via inhibition on MAPK signalling. J Cell Mol Med *23*, 7010–7020. 10.1111/JCMM.14588.

983 11. Bastide, A., Peretti, D., Knight, J.R.P., Grosso, S., Spriggs, R. V., Pichon, X., Sbarrato, T., Roobol,
984 A., Roobol, J., Vito, D., et al. (2017). RTN3 Is a Novel Cold-Induced Protein and Mediates
985 Neuroprotective Effects of RBM3. Current Biology *27*, 638. 10.1016/J.CUB.2017.01.047.

986 12. Chip, S., Zelmer, A., Ogunshola, O.O., Felderhoff-Mueser, U., Nitsch, C., Bührer, C., and
987 Wellmann, S. (2011). The RNA-binding protein RBM3 is involved in hypothermia induced
988 neuroprotection. Neurobiol Dis *43*, 388–396. 10.1016/j.nbd.2011.04.010.

989 13. Peretti, D., Bastide, A., Radford, H., Verity, N., Molloy, C., Martin, M.G., Moreno, J.A., Steinert,
990 J.R., Smith, T., Dinsdale, D., et al. (2015). RBM3 mediates structural plasticity and protective

991 effects of cooling in neurodegeneration. Nature 2015 518:7538 *518*, 236–239.
992 10.1038/nature14142.

993 14. Wierstra, I. (2008). Sp1: Emerging roles—Beyond constitutive activation of TATA-less
994 housekeeping genes. Biochem Biophys Res Commun *372*, 1–13. 10.1016/J.BBRC.2008.03.074.

995 15. Sumitomo, Y., Higashitsuji, H., Higashitsuji, H., Liu, Y., Fujita, T., Sakurai, T., Candeias, M.M.,
996 Itoh, K., Chiba, T., and Fujita, J. (2012). Identification of a novel enhancer that binds Sp1 and
997 contributes to induction of cold-inducible RNA-binding protein (cirp) expression in
998 mammalian cells. BMC Biotechnol *12*, 72. 10.1186/1472-6750-12-72.

999 16. Gomez-Pastor, R., Burchfiel, E.T., and Thiele, D.J. (2018). Regulation of heat shock
1000 transcription factors and their roles in physiology and disease. Nat Rev Mol Cell Biol *19*, 4–19.
1001 10.1038/NRM.2017.73.

1002 17. Sanjana, N.E., Shalem, O., and Zhang, F. Improved vectors and genome - wide libraries for
1003 CRISPR screening.

1004 18. Shalem, O., Sanjana, N.E., Hartenian, E., Shi, X., Scott, D.A., Mikkelson, T., Heckl, D., Ebert, B.L.,
1005 Root, D.E., Doench, J.G., et al. (2014). Genome-scale CRISPR-Cas9 knockout screening in
1006 human cells. Science *343*, 84–87. 10.1126/science.1247005.

1007 19. Joung, J., Konermann, S., Gootenberg, J.S., Abudayyeh, O.O., Platt, R.J., Brigham, M.D.,
1008 Sanjana, N.E., and Zhang, F. (2017). Genome-scale CRISPR-Cas9 knockout and transcriptional
1009 activation screening. Nat Protoc *12*, 828–863. 10.1038/nprot.2017.016.

1010 20. McIntyre, S., Nelson, K.B., Mulkey, S.B., Lechpammer, M., Molloy, E., and Badawi, N. (2021).
1011 Neonatal encephalopathy: Focus on epidemiology and underexplored aspects of etiology.
1012 Semin Fetal Neonatal Med *26*. 10.1016/J.SINY.2021.101265.

1013 21. Geneva, I.I., Cuzzo, B., Fazili, T., and Javaid, W. (2019). Normal Body Temperature: A
1014 Systematic Review. Open Forum Infect Dis *6*. 10.1093/OFID/OFZ032.

1015 22. Knight, J.R.P., Bastide, A., Roobol, A., Roobol, J., Jackson, T.J., Utami, W., Barrett, D.A., Smales,
1016 C.M., and Willis, A.E. (2015). Eukaryotic elongation factor 2 kinase regulates the cold stress
1017 response by slowing translation elongation. Biochem J *465*, 227–238. 10.1042/BJ20141014.

1018 23. Shaw, G., Morse, S., Ararat, M., and Graham, F.L. (2002). Preferential transformation of
1019 human neuronal cells by human adenoviruses and the origin of HEK 293 cells. The FASEB
1020 Journal. 10.1096/fj.01-0995fje.

1021 24. Barnes, E.N., Biedler, J.L., Spengler, B.A., and Lyser, K.M. (1981). The fine structure of
1022 continuous human neuroblastoma lines SK-N-SH, SK-N-BE(2), and SK-N-MC. In Vitro *17*, 619–
1023 631. 10.1007/BF02618461.

1024 25. Stepanenko, A.A., and Dmitrenko, V. V (2015). HEK293 in cell biology and cancer research:
1025 phenotype, karyotype, tumorigenicity, and stress-induced genome-phenotype evolution.
1026 Gene *569*, 182–190. 10.1016/j.gene.2015.05.065.

1027 26. Jackson, T.C., Manole, M.D., Kotermanski, S.E., Jackson, E.K., Clark, R.S.B., and Kochanek, P.M.
1028 (2015). Cold stress protein RBM3 responds to temperature change in an ultra-sensitive
1029 manner in young neurons. Neuroscience *305*, 268–278. 10.1016/j.neuroscience.2015.08.012.

1030 27. Hartmann, J., Haap, M., Kopp, H.-G., and Lipp, H.-P. (2009). Tyrosine kinase inhibitors - a
1031 review on pharmacology, metabolism and side effects. Curr Drug Metab *10*, 470–481.
1032 10.2174/138920009788897975.

1033 28. Nelson, V., Ziehr, J., Agulnik, M., and Johnson, M. (2013). Afatinib: emerging next-generation
1034 tyrosine kinase inhibitor for NSCLC. Onco Targets Ther *6*, 135–143. 10.2147/OTT.S23165.

1035 29. Kim, T.M., Lee, K.W., Oh, D.Y., Lee, J.S., Im, S.A., Kim, D.W., Han, S.W., Kim, Y.J., Kim, T.Y., Kim,
1036 J.H., et al. (2018). Phase 1 Studies of Poziotinib, an Irreversible Pan-HER Tyrosine Kinase
1037 Inhibitor in Patients with Advanced Solid Tumors. Cancer Res Treat *50*, 835–842.
1038 10.4143/CRT.2017.303.

1039 30. Erber, R., Thurnher, A., Katsen, A.D., Groth, G., Kerger, H., Hammes, H.P., Menger, M.D.,
1040 Ullrich, A., and Vajkoczy, P. (2004). Combined inhibition of VEGF and PDGF signaling enforces
1041 tumor vessel regression by interfering with pericyte-mediated endothelial cell survival
1042 mechanisms. FASEB J *18*, 338–340. 10.1096/FJ.03-0271FJE.

1043 31. Lee, H., Kim, J.W., Choi, D.K., Yu, J.H., Kim, J.H., Lee, D.S., and Min, S.H. (2020). Poziotinib
1044 suppresses ovarian cancer stem cell growth via inhibition of HER4-mediated STAT5 pathway.
1045 Biochem Biophys Res Commun *526*, 158–164. 10.1016/J.BBRC.2020.03.046.

1046 32. Grinstein, E., Jundt, F., Weinert, I., Wernet, P., and Royer, H.D. (2002). Sp1 as G1 cell cycle
1047 phase specific transcription factor in epithelial cells. Oncogene 2002 21:10 *21*, 1485–1492.
1048 10.1038/sj.onc.1205211.

1049 33. Li, W., Xu, H., Xiao, T., Cong, L., Love, M.I., Zhang, F., Irizarry, R.A., Liu, J.S., Brown, M., and Liu,
1050 X.S. (2014). MAGeCK enables robust identification of essential genes from genome-scale
1051 CRISPR/Cas9 knockout screens. Genome Biol *15*, 554. 10.1186/s13059-014-0554-4.

1052 34. Tan, N.Y., and Khachigian, L.M. (2009). Sp1 phosphorylation and its regulation of gene
1053 transcription. Mol Cell Biol *29*, 2483–2488. 10.1128/mcb.01828-08.

1054 35. Nagai, G., and Nakaoka, Y. (1998). Cooling sensitive [Ca2+](i) response associated with
1055 signaling of G protein-coupled receptors. Biochem Biophys Res Commun *248*, 733–737.
1056 10.1006/BBRC.1998.8873.

1057 36. Chelban, V., Patel, N., Vandrovcova, J., Zanetti, M.N., Lynch, D.S., Ryten, M., Botía, J.A., Bello,
1058 O., Tribollet, E., Efthymiou, S., et al. (2017). Mutations in NKX6-2 Cause Progressive Spastic
1059 Ataxia and Hypomyelination. Am J Hum Genet *100*, 969–977. 10.1016/J.AJHG.2017.05.009.

1060 37. ZNF260 zinc finger protein 260 [Homo sapiens (human)] - Gene - NCBI
1061 https://www.ncbi.nlm.nih.gov/gene?Db=gene&Cmd=DetailsSearch&Term=339324#gene-
1062 expression.

1063 38. Burke, T.L., and Grant, P.A. (2009). Histone Acetylation Complexes. Handbook of Cell
1064 Signaling, Second Edition *3*, 2369–2378. 10.1016/B978-0-12-374145-5.00285-0.

1065 39. Zhou, X., Shang, Y.N., Lu, R., Fan, C.W., and Mo, X.M. (2019). High ANKZF1 expression is
1066 associated with poor overall survival and recurrence-free survival in colon cancer.
1067 https://doi.org/10.2217/fon-2018-0920 *15*, 2093–2106. 10.2217/FON-2018-0920.

1068 40. Tawamie, H., Martianov, I., Wohlfahrt, N., Buchert, R., Mengus, G., Uebe, S., Janiri, L., Hirsch,
1069 F.W., Schumacher, J., Ferrazzi, F., et al. (2017). Hypomorphic Pathogenic Variants in TAF13 Are
1070 Associated with Autosomal-Recessive Intellectual Disability and Microcephaly. Am J Hum
1071 Genet *100*, 555. 10.1016/J.AJHG.2017.01.032.

1072 41. ZNF71 zinc finger protein 71 [Homo sapiens (human)] - Gene - NCBI
1073 https://www.ncbi.nlm.nih.gov/gene?Db=gene&Cmd=DetailsSearch&Term=58491.

1074 42. Yu, H. V., Tao, L., Llamas, J., Wang, X., Nguyen, J.D., Trecek, T., and Segil, N. (2021). POU4F3
1075 pioneer activity enables ATOH1 to drive diverse mechanoreceptor differentiation through a
1076 feed-forward epigenetic mechanism. Proc Natl Acad Sci U S A *118*.
1077 10.1073/PNAS.2105137118/-/DCSUPPLEMENTAL.

1078 43. GATAD2A GATA zinc finger domain containing 2A [Homo sapiens (human)] - Gene - NCBI
1079 https://www.ncbi.nlm.nih.gov/gene/54815.

1080 44. Zhang, Y., Fang, Y., Tang, Y., Han, S., Jia, J., Wan, X., Chen, J., Yuan, Y., Zhao, B., and Fang, D.
1081 (2022). SMYD5 catalyzes histone H3 lysine 36 trimethylation at promoters. Nature
1082 Communications 2022 13:1 *13*, 1–19. 10.1038/s41467-022-30940-1.

1083 45. Kidder, B.L., He, R., Wangsa, D., Padilla-Nash, H.M., Bernardo, M.M., Sheng, S., Ried, T., and
1084 Zhao, K. (2017). SMYD5 Controls Heterochromatin and Chromosome Integrity during
1085 Embryonic Stem Cell Differentiation. Cancer Res *77*, 6729–6745. 10.1158/0008-5472.CAN-17-
1086 0828.

1087 46. Murphy, M.W., Sarver, A.L., Rice, D., Hatzi, K., Ye, K., Melnick, A., Heckert, L.L., Zarkower, D.,
1088 and Bardwell, V.J. (2010). Genome-wide analysis of DNA binding and transcriptional
1089 regulation by the mammalian Doublesex homolog DMRT1 in the juvenile testis. Proc Natl
1090 Acad Sci U S A *107*, 13360–13365. 10.1073/PNAS.1006243107/SUPPL_FILE/SD01.XLS.

1091 47. Weber, C., Zhou, Y., Lee, J.G., Looger, L.L., Qian, G., Ge, C., and Capel, B. (2020). Temperature-
1092 dependent sex determination is mediated by pSTAT3 repression of Kdm6b. Science (1979)
1093 *368*, 303–306. 10.1126/SCIENCE.AAZ4165/SUPPL_FILE/AAZ4165_S1.MP4.

1094 48. Kim, D.H., Doyle, M.R., Sung, S., and Amasino, R.M. (2009). Vernalization: winter and the
1095 timing of flowering in plants. Annu Rev Cell Dev Biol *25*, 277–299.
1096 10.1146/annurev.cellbio.042308.113411.

1097 49. Fellous, A., Earley, R.L., and Silvestre, F. (2019). The Kdm/Kmt gene families in the self-
1098 fertilizing mangrove rivulus fish, Kryptolebias marmoratus, suggest involvement of histone
1099 methylation machinery in development and reproduction. Gene *687*, 173–187.
1100 10.1016/J.GENE.2018.11.046.

1101 50. Youn, J.Y., Dyakov, B.J.A., Zhang, J., Knight, J.D.R., Vernon, R.M., Forman-Kay, J.D., and
1102 Gingras, A.C. (2019). Properties of Stress Granule and P-Body Proteomes. Mol Cell *76*, 286–
1103 294. 10.1016/J.MOLCEL.2019.09.014.

1104 51. Aljazi, M.B., Gao, Y., Wu, Y., and He, J. (2022). SMYD5 is a histone H3-specific
1105 methyltransferase mediating mono-methylation of histone H3 lysine 36 and 37. Biochem
1106 Biophys Res Commun *599*, 142–147. 10.1016/J.BBRC.2022.02.043.

1107 52. Diaz, J., Abiola, S., Kim, N., Avaritt, O., Flock, D., Yu, J., Northington, F.J., and Chavez-Valdez, R.
1108 (2017). Therapeutic hypothermia provides variable protection against behavioral deficits after
1109 neonatal HI: A potential role for BDNF. Dev Neurosci *39*, 257. 10.1159/000454949.

1110 53. Xi, Y., Park, S.R., Kim, D.H., Kim, E.D., and Sung, S. (2020). Transcriptome and epigenome
1111 analyses of vernalization in Arabidopsis thaliana. Plant J *103*, 1490. 10.1111/TPJ.14817.

1112 54. Fan, L., Lesser, A.F., Sweet, D.R., Keerthy, K.S., Lu, Y., Chan, E.R., Vinayachandran, V., Ilkayeva,
1113 O., Das, T., Newgard, C.B., et al. (2022). KLF15 controls brown adipose tissue transcriptional
1114 flexibility and metabolism in response to various energetic demands. iScience *25*, 105292.
1115 10.1016/J.ISCI.2022.105292.

1116 55. Katano-Toki, A., Satoh, T., Tomaru, T., Yoshino, S., Ishizuka, T., Ishii, S., Ozawa, A., Shibusawa,
1117 N., Tsuchiya, T., Saito, T., et al. (2013). THRAP3 Interacts with HELZ2 and Plays a Novel Role in
1118 Adipocyte Differentiation. Molecular Endocrinology *27*, 769. 10.1210/ME.2012-1332.

1119 56. THRAP3 thyroid hormone receptor associated protein 3 [Homo sapiens (human)] - Gene -
1120 NCBI https://www.ncbi.nlm.nih.gov/gene?Db=gene&Cmd=DetailsSearch&Term=9967.

1121 57. Guo, K., Searfoss, G., Krolikowski, D., Pagnoni, M., Franks, C., Clark, K., Yu, K.T., Jaye, M., and
1122 Ivashchenko, Y. (2001). Hypoxia induces the expression of the pro-apoptotic gene BNIP3. Cell
1123 Death Differ *8*, 367–376. 10.1038/SJ.CDD.4400810.

1124 58. Abdel-Wahab, O., Adli, M., LaFave, L.M., Gao, J., Hricik, T., Shih, A.H., Pandey, S., Patel, J.P.,
1125 Chung, Y.R., Koche, R., et al. (2012). ASXL1 mutations promote myeloid transformation
1126 through loss of PRC2-mediated gene repression. Cancer Cell *22*, 180–193.
1127 10.1016/J.CCR.2012.06.032.

1128 59. Kaakkola, S. (2000). Clinical pharmacology, therapeutic use and potential of COMT inhibitors
1129 in Parkinson's disease. Drugs *59*, 1233–1250. 10.2165/00003495-200059060-00004.

1130 60. Feng, Z., Saha, L., Dritsa, C., Wan, Q., and Glebov, O.O. (2022). Temperature-dependent
1131 structural plasticity of hippocampal synapses. Front Cell Neurosci *16*, 520.
1132 10.3389/FNCEL.2022.1009970/BIBTEX.

1133 61. Carvelli, L., Blakely, R.D., and DeFelice, L.J. (2008). Dopamine transporter/syntaxin 1A
1134 interactions regulate transporter channel activity and dopaminergic synaptic transmission.
1135 Proc Natl Acad Sci U S A *105*, 14192–14197. 10.1073/PNAS.0802214105.

1136 62. Gao, H., Chakraborty, G., Lee-Lim, A.P., Mavrakis, K.J., Wendel, H.G., and Giancotti, F.G.
1137 (2014). Forward genetic screens in mice uncover mediators and suppressors of metastatic

1138 reactivation. Proc Natl Acad Sci U S A *111*, 16532–16537.
1139 10.1073/PNAS.1403234111/SUPPL_FILE/PNAS.201403234SI.PDF.

1140 63. INDACOCHEA, A., GUERRERO, S., UREÑA, M., ARAUJO, F., COLL, O., LLEONART, M.E., and
1141 GEBAUER, F. (2021). Cold-inducible RNA binding protein promotes breast cancer cell
1142 malignancy by regulating Cystatin C levels. RNA *27*, 190–201. 10.1261/RNA.076422.120.

1143 64. Nicolas, M., Noe, V., Jensen, K., and Ciudad CJ (2001). Cloning and characterization of the 5'-
1144 flanking region of the human transcription factor Sp1 gene. . J Biol Chem, 22126-22132.

1145 65. Yang, F., Eckardt, S., Leu, N.A., McLaughlin, K.J., and Wang, P.J. (2008). Mouse TEX15 is
1146 essential for DNA double-strand break repair and chromosomal synapsis during male meiosis.
1147 J Cell Biol *180*, 673. 10.1083/JCB.200709057.

1148 66. TEX15 testis expressed 15, meiosis and synapsis associated [Homo sapiens (human)] - Gene -
1149 NCBI https://www.ncbi.nlm.nih.gov/gene/56154.

1150 67. Hanna, C.W., Huang, J., Belton, C., Reinhardt, S., Dahl, A., Andrews, S., Francis Stewart, A.,
1151 Kranz, A., and Kelsey, G. (2022). Loss of histone methyltransferase SETD1B in oogenesis
1152 results in the redistribution of genomic histone 3 lysine 4 trimethylation. Nucleic Acids Res *50*,
1153 1993. 10.1093/NAR/GKAC051.

1154 68. Pajoro, A., Severing, E., Angenent, G.C., and Immink, R.G.H. (2017). Histone H3 lysine 36
1155 methylation affects temperature-induced alternative splicing and flowering in plants. Genome
1156 Biol *18*, 1–12. 10.1186/S13059-017-1235-X/FIGURES/4.

1157 69. Michaels, K.K., Mostafa, S.M., Capella, J.R., and Moore, C.L. (2020). Regulation of alternative
1158 polyadenylation in the yeast Saccharomyces cerevisiae by histone H3K4 and H3K36
1159 methyltransferases. Nucleic Acids Res *48*, 5407–5425. 10.1093/NAR/GKAA292.

1160 70. Xu, S.J., Lombroso, S.I., Fischer, D.K., Carpenter, M.D., Marchione, D.M., Hamilton, P.J., Lim,
1161 C.J., Neve, R.L., Garcia, B.A., Wimmer, M.E., et al. (2021). Chromatin-mediated alternative
1162 splicing regulates cocaine-reward behavior. Neuron *109*, 2943-2966.e8.
1163 10.1016/J.NEURON.2021.08.008.

1164 71. Preußner, M., Goldammer, G., Neumann, A., Haltenhof, T., Rautenstrauch, P., Müller-
1165 McNicoll, M., and Heyd, F. (2017). Body Temperature Cycles Control Rhythmic Alternative
1166 Splicing in Mammals. Mol Cell *67*, 433-446.e4. 10.1016/J.MOLCEL.2017.06.006.

1167 72. Horii, Y., Shiina, T., Uehara, S., Nomura, K., Shimaoka, H., Horii, K., and Shimizu, Y. (2019).
1168 Hypothermia induces changes in the alternative splicing pattern of cold-inducible RNA-binding
1169 protein transcripts in a non-hibernator, the mouse. Biomed Res *40*, 153–161.
1170 10.2220/BIOMEDRES.40.153.

1171 73. Sano, Y., Shiina, T., Naitou, K., Nakamori, H., and Shimizu, Y. (2015). Hibernation-specific
1172 alternative splicing of the mRNA encoding cold-inducible RNA-binding protein in the hearts of
1173 hamsters. Biochem Biophys Res Commun *462*, 322–325. 10.1016/j.bbrc.2015.04.135.

1174 74. Smart, F., Aschrafi, A., Atkins, A., Owens, G.C., Pilotte, J., Cunningham, B.A., and Vanderklish,
1175 P.W. (2007). Two isoforms of the cold-inducible mRNA-binding protein RBM3 localize to
1176 dendrites and promote translation. J Neurochem *101*, 1367–1379. 10.1111/J.1471-
1177 4159.2007.04521.X.

1178 75. Al-Fageeh, M.B., and Smales, C.M. (2013). Alternative promoters regulate cold inducible RNA-
1179 binding (CIRP) gene expression and enhance transgene expression in mammalian cells. Mol
1180 Biotechnol *54*, 238–249. 10.1007/s12033-013-9649-5.

1181 76. Nicolas, M., Noe, V., Jensen, K.B., and Ciudad, C.J. (2001). Cloning and characterization of the
1182 5'-flanking region of the human transcription factor Sp1 gene. J Biol Chem *276*, 22126–22132.
1183 10.1074/jbc.M010740200.

1184 77. Chambers, S.M., Fasano, C.A., Papapetrou, E.P., Tomishima, M., Sadelain, M., Studer, L., and
1185 Author, N.B. (2009). Highly efficient neural conversion of human ES and iPS cells by dual
1186 inhibition of SMAD signaling HHS Public Access Author manuscript. Nat Biotechnol *27*, 275–
1187 280. 10.1038/nbt.1529.

1188 78. Xiang, J., Wan, C., Guo, R., and Guo, D. (2016). Is Hydrogen Peroxide a Suitable Apoptosis
1189 Inducer for All Cell Types? Biomed Res Int *2016*. 10.1155/2016/7343965.

1190 79. Cell cycle staining with Propidium Iodide for the cytoplasmic GFP transfected cells using
1191 Paraformaldehyde and Ethanol (2010). 1–2. https://flowcyt.rutgers.edu/wp-
1192 content/uploads/2017/10/Cell-cycle-staining-with-PI-for-GFP-transfected-cells-using-
1193 PFA_EtOH_2.pdf.

1194 80. Kutner, R.H., Zhang, X.Y., and Reiser, J. (2009). Production, concentration and titration of
1195 pseudotyped HIV-1-based lentiviral vectors. Nat Protoc *4*, 495–505. 10.1038/nprot.2009.22.

1196 81. Wang, B., Wang, M., Zhang, W., Xiao, T., Chen, C.H., Wu, A., Wu, F., Traugh, N., Wang, X., Li,
1197 Z., et al. (2019). Integrative analysis of pooled CRISPR genetic screens using MAGeCKFlute. Nat
1198 Protoc *14*, 756–780. 10.1038/s41596-018-0113-7.

1199 82. Statistical R Core Team (2017). R Foundation for Statistical Computing Vienna Austria. R: A
1200 language and environment for computing.

1201 83. 4×Lentivirus Concentrator Solution https://www.mdanderson.org/documents/core-
1202 facilities/Functional%20Genomics%20Core/Homemade%204fold%20lentivirus%20concentrat
1203 or.pdf.

1204 84. Rueden, C.T., Schindelin, J., Hiner, M.C., DeZonia, B.E., Walter, A.E., Arena, E.T., and Eliceiri,
1205 K.W. (2017). ImageJ2: ImageJ for the next generation of scientific image data. BMC
1206 Bioinformatics *18*, 1–26. 10.1186/S12859-017-1934-Z/FIGURES/7.

1207 85. Schindelin, J., Arganda-Carreras, I., Frise, E., Kaynig, V., Longair, M., Pietzsch, T., Preibisch, S.,
1208 Rueden, C., Saalfeld, S., Schmid, B., et al. (2012). Fiji: an open-source platform for biological-
1209 image analysis. Nature Methods 2012 9:7 *9*, 676–682. 10.1038/nmeth.2019.

1210 86. Stirling, D.R., Swain-Bowden, M.J., Lucas, A.M., Carpenter, A.E., Cimini, B.A., and Goodman, A.
1211 (2021). CellProfiler 4: improvements in speed, utility and usability. BMC Bioinformatics *22*.
1212 10.1186/S12859-021-04344-9.

1213 87. Fortin, J.P., Triche, T.J., and Hansen, K.D. (2017). Preprocessing, normalization and integration
1214 of the Illumina HumanMethylationEPIC array with minfi. Bioinformatics *33*, 558.
1215 10.1093/BIOINFORMATICS/BTW691.

1216 88. Triche, T.J., Weisenberger, D.J., Van Den Berg, D., Laird, P.W., and Siegmund, K.D. (2013). Low-
1217 level processing of Illumina Infinium DNA Methylation BeadArrays. Nucleic Acids Res *41*, e90.
1218 10.1093/NAR/GKT090.

1219 89. Aryee, M.J., Jaffe, A.E., Corrada-Bravo, H., Ladd-Acosta, C., Feinberg, A.P., Hansen, K.D., and
1220 Irizarry, R.A. (2014). Minfi: a flexible and comprehensive Bioconductor package for the
1221 analysis of Infinium DNA methylation microarrays. Bioinformatics *30*, 1363.
1222 10.1093/BIOINFORMATICS/BTU049.

1223 90. Leek, J.T., Johnson, W.E., Parker, H.S., Jaffe, A.E., and Storey, J.D. (2012). The sva package for
1224 removing batch effects and other unwanted variation in high-throughput experiments.
1225 Bioinformatics *28*, 882. 10.1093/BIOINFORMATICS/BTS034.

1226 91. Ritchie, M.E., Phipson, B., Wu, D., Hu, Y., Law, C.W., Shi, W., and Smyth, G.K. (2015). limma
1227 powers differential expression analyses for RNA-sequencing and microarray studies. Nucleic
1228 Acids Res *43*, e47. 10.1093/NAR/GKV007.

1229 92. CUT&RUN Protocol v1.7 (2021).
1230 https://www.epicypher.com/content/documents/protocols/cutana-cut&run-
1231 protocol_1.7.pdf.

1232 93. Kong, N.R., Chai, L., Tenen, D.G., and Bassal, M.A. (2021). A modified CUT&RUN protocol and
1233 analysis pipeline to identify transcription factor binding sites in human cell lines. STAR Protoc
1234 *2*. 10.1016/J.XPRO.2021.100750.

1235 94. Martin, M. (2011). Cutadapt removes adapter sequences from high-throughput sequencing
1236 reads. EMBnet J *17*, 10–12. 10.14806/EJ.17.1.200.

1237 95. Langmead, B., and Salzberg, S.L. (2012). Fast gapped-read alignment with Bowtie 2. Nat
1238 Methods *9*, 357–359. 10.1038/nmeth.1923.

1239 96. Li, H., Handsaker, B., Wysoker, A., Fennell, T., Ruan, J., Homer, N., Marth, G., Abecasis, G., and
1240 Durbin, R. (2009). The Sequence Alignment/Map format and SAMtools. Bioinformatics *25*,
1241 2078–2079. 10.1093/BIOINFORMATICS/BTP352.

1242 97. Luo, Y., Hitz, B.C., Gabdank, I., Hilton, J.A., Kagda, M.S., Lam, B., Myers, Z., Sud, P., Jou, J., Lin,
1243 K., et al. (2020). New developments on the Encyclopedia of DNA Elements (ENCODE) data
1244 portal. Nucleic Acids Res *48*, D882–D889. 10.1093/NAR/GKZ1062.

1245 98. Quinlan, A.R., and Hall, I.M. (2010). BEDTools: a flexible suite of utilities for comparing
1246 genomic features. Bioinformatics *26*, 841–842. 10.1093/BIOINFORMATICS/BTQ033.

1247 99. Meers, M.P., Tenenbaum, D., and Henikoff, S. (2019). Peak calling by Sparse Enrichment
1248 Analysis for CUT&RUN chromatin profiling. Epigenetics Chromatin *12*, 1–11. 10.1186/S13072-
1249 019-0287-4/FIGURES/6.

1250 100. Stark, R., and Brown, G. (2012). DiffBind : differential binding analysis of ChIP-Seq peak data.

1251 101. Yu, G., Wang, L.G., and He, Q.Y. (2015). ChIPseeker: an R/Bioconductor package for ChIP peak
1252 annotation, comparison and visualization. Bioinformatics *31*, 2382–2383.
1253 10.1093/BIOINFORMATICS/BTV145.

1254 102. Team BC, and Maintainer BP (2019). TxDb.Hsapiens.UCSC.hg38.knownGene: Annotation
1255 package for TxDb object(s).

1256 103. Carlson M (2019). org.Hs.eg.db: Genome wide annotation for Human. .

1257 104. Ramírez, F., Dündar, F., Diehl, S., Grüning, B.A., and Manke, T. (2014). deepTools: a flexible
1258 platform for exploring deep-sequencing data. Nucleic Acids Res *42*, W187.
1259 10.1093/NAR/GKU365.

1260 105. Bernas, S.N., Leiter, O., Walker, T.L., and Kempermann, G. (2017). Isolation, Culture and
1261 Differentiation of Adult Hippocampal Precursor Cells. Bio Protoc *7*.
1262 10.21769/BIOPROTOC.2603.

1263 106. Soneson, C., Love, M.I., and Robinson, M.D. (2016). Differential analyses for RNA-seq:
1264 Transcript-level estimates improve gene-level inferences. F1000Res *4*.
1265 10.12688/F1000RESEARCH.7563.2/DOI.

1266 107. Team BC, and Maintainer BP (2016). TxDb.Mmusculus.UCSC.mm10.ensGene: Annotation
1267 package for TxDb object(s)..

1268 108. Love, M.I., Huber, W., and Anders, S. (2014). Moderated estimation of fold change and
1269 dispersion for RNA-seq data with DESeq2. Genome Biol *15*, 1–21. 10.1186/S13059-014-0550-
1270 8/FIGURES/9.

1271 109. Shen L, and Sinai ISoMaM (2022). GeneOverlap: Test and visualize gene overlaps. .

1272 110. Subramanian, A., Tamayo, P., Mootha, V.K., Mukherjee, S., Ebert, B.L., Gillette, M.A.,
1273 Paulovich, A., Pomeroy, S.L., Golub, T.R., Lander, E.S., et al. (2005). Gene set enrichment
1274 analysis: a knowledge-based approach for interpreting genome-wide expression profiles. Proc
1275 Natl Acad Sci U S A *102*, 15545–15550. 10.1073/PNAS.0506580102.

1276 111. Mootha, V.K., Lindgren, C.M., Eriksson, K.F., Subramanian, A., Sihag, S., Lehar, J., Puigserver,
1277 P., Carlsson, E., Ridderstråle, M., Laurila, E., et al. (2003). PGC-1alpha-responsive genes
1278 involved in oxidative phosphorylation are coordinately downregulated in human diabetes. Nat
1279 Genet *34*, 267–273. 10.1038/NG1180.

1280 112. Liberzon, A., Birger, C., Thorvaldsdóttir, H., Ghandi, M., Mesirov, J.P., and Tamayo, P. (2015).
1281 The Molecular Signatures Database (MSigDB) hallmark gene set collection. Cell Syst *1*, 417–
1282 425. 10.1016/J.CELS.2015.12.004.